CDC20B is required for deuterosome-mediated centriole production in 1 multiciliated cells

Diego R Revinski, Laure-Emmanuelle Zaragosi, Camille Boutin, Marie Deprez, Virginie Thomé, Olivier Rosnet, Anne-Sophie Gay, Agnès Paquet, Nicolas Pons, Gilles Ponzio, et al.

▶ **To cite this version:**

Diego R Revinski, Laure-Emmanuelle Zaragosi, Camille Boutin, Marie Deprez, Virginie Thomé, et al.. CDC20B is required for deuterosome-mediated centriole production in 1 multiciliated cells. Nature Communications, 2018, 9, pp.4668. 10.1038/s41467-018-06768-z . hal-02064869

HAL Id: hal-02064869
https://hal.science/hal-02064869

Submitted on 12 Mar 2019

HAL is a multi-disciplinary open access archive for the deposit and dissemination of scientific research documents, whether they are published or not. The documents may come from teaching and research institutions in France or abroad, or from public or private research centers.

L'archive ouverte pluridisciplinaire **HAL**, est destinée au dépôt et à la diffusion de documents scientifiques de niveau recherche, publiés ou non, émanant des établissements d'enseignement et de recherche français ou étrangers, des laboratoires publics ou privés.

Title: CDC20B is required for deuterosome-mediated centriole production in multiciliated cells

Authors: Diego R. Revinski[1†], Laure-Emmanuelle Zaragosi[2†], Camille Boutin[1†], Sandra Ruiz-Garcia[2], Marie Deprez[2], Virginie Thomé[1], Olivier Rosnet[1], Anne-Sophie Gay[2], Olivier Mercey[2], Agnès Paquet[2], Nicolas Pons[2], Gilles Ponzio[2], Brice Marcet[2*], Laurent Kodjabachian[1*], Pascal Barbry[2*]

Affiliations:

[1] Aix Marseille Univ, CNRS, IBDM, Marseille, France

[2] Université Côte d'Azur, CNRS, IPMC, Sophia-Antipolis, France.

[†] These authors contributed equally

[*]Correspondence to: marcet@ipmc.cnrs.fr; laurent.kodjabachian@univ-amu.fr; barbry@ipmc.cnrs.fr

Keywords: multiciliated cell, centriole, deuterosome, motile cilia, CDC20B, Separase, PLK1, cell cycle, *Xenopus*, mouse, human

Abstract: Multiciliated cells (MCCs) harbour dozens to hundreds of motile cilia, which generate hydrodynamic forces important in animal physiology. In vertebrates, MCC differentiation involves massive centriole production by poorly characterized structures called deuterosomes. Here, single-cell RNA sequencing reveals that human deuterosome-stage MCCs are characterized by the expression of many cell cycle-related genes. We further investigated the uncharacterized vertebrate-specific *cell division cycle 20B* (*CDC20B*) gene, which hosts microRNA-449abc. We show that CDC20B protein associates to deuterosomes and is required for centriole release and subsequent cilia production in mouse and *Xenopus* MCCs. CDC20B interacts with PLK1, a kinase known to coordinate centriole disengagement with the protease Separase in mitotic cells. Strikingly, over-expression of Separase rescues centriole disengagement and cilia production in CDC20B-deficient MCCs. This work reveals the shaping of a new biological function, deuterosome-mediated centriole production in vertebrate MCCs, by adaptation of canonical and recently evolved cell cycle-related molecules.

Introduction

Multiciliated cells (MCCs) are present throughout metazoan evolution and serve functions ranging from locomotion of marine larvae and flatworms, to brain homeostasis, mucociliary clearance of pathogens and transportation of oocytes in vertebrates[1-3]. The formation of MCCs requires the production of numerous motile cilia through a complex process called multiciliogenesis[2, 3]. The transcriptional control of multiciliogenesis has been decrypted to a large extent, through studies in *Xenopus* and mouse[2]. Seating at the top of the cascade, the Geminin-related factors GemC1[4-7] and Multicilin[8, 9] (MCIDAS in mammals) are both necessary and sufficient to initiate MCC differentiation. GemC1 and Multicilin in complex with E2F transcription factors have been reported to activate the expression of Myb, FoxJ1,

Rfx2 and Rfx3, which collectively regulate the expression of a large body of effectors required for the formation of multiple motile cilia[4, 5, 8-11]. Recently, defective multiciliogenesis caused by mutations in MCIDAS and Cyclin O (CCNO) has been associated with congenital respiratory and fertility syndromes in human[12, 13].

Each cilium sits atop a modified centriole, called a basal body (BB). After they exit from the cell cycle, maturing MCCs face the challenge of producing dozens to hundreds of centrioles in a limited time window. In vertebrate MCCs, bulk centriole biogenesis is mostly achieved through an acentriolar structure named the deuterosome, although canonical amplification from parental centrioles also occurs[1-3]. The deuterosome was first described in early electron microscopy studies of various multiciliated tissues including the mammalian lung[14] and oviduct[15, 16], the avian trachea[17], and the *Xenopus* tadpole epidermis and trachea[18]. In mammalian MCCs, the deuterosome was described as a spherical mass of fibers organized into an inner dense region and an outer, more delicate, corona[16]. In *Xenopus*, deuterosomes were initially named procentriole organizers and were reported as dense amorphous masses[18]. Recent studies have revealed that deuterosome-mediated centriole synthesis mobilizes key components of the centriole-dependent duplication pathway of the cell cycle, including CEP152, PLK4 and SAS6[19-21]. However, the deuterosome itself differs from the centriole and may contain specific components. The identification of one such component, called DEUP1 for Deuterosome assembly protein 1, opened the possibility to investigate the deuterosome at the molecular level[21]. In mouse tracheal ependymal cells, DEUP1 was detected in the core of the deuterosome[21]. DEUP1, also known as CCDC67, is a conserved vertebrate paralogue of CEP63, itself known for its importance in initiation of centriole duplication during the cell cycle[21, 22]. Consistently, DEUP1 was shown to be essential for centriole multiplication in mouse and *Xenopus* MCCs[21]. Both CEP63 and DEUP1 interact with CEP152, an essential event for centriole duplication and multiplication in cycling cells and MCCs, respectively[21, 22].

Once centriole multiplication is over, neo-synthesized centrioles must disengage from deuterosomes and parental centrioles, convert into BBs and migrate apically to dock at the plasma membrane to initiate cilium elongation.

In this study, we aimed at better understanding deuterosome biology. We found that the gene *CDC20B* was specifically expressed in maturing MCCs during the phase of centriole multiplication. We established the corresponding CDC20B protein as an essential regulator of centriole-deuterosome disengagement. This work illustrates well the strong functional relationships that exist between centriole release from deuterosomes and centriole disengagement in mitotic cells. It also posits CDC20B as a new component of a "multiciliary locus" that contains several gene products, either proteins, such as MCIDAS, CCNO or CDC20B itself, or microRNAs, such as miR-449abc, which are all actively involved into multiciliogenesis.

Results

MCC single-cell transcriptome at deuterosome-stage

To identify new regulators of centriole multiplication, we analyzed the transcriptome of human airway epithelial cells (HAECs) at the differentiation stage corresponding to active centriole multiplication[23] at the single-cell level (Fig. 1a). Gene expression data from 1663 cells was projected on a 2D space by *t*-distributed Stochastic Neighbor Embedding (tSNE) (Fig. 1b). We identified a small group of 37 cells corresponding to maturing MCCs engaged in deuterosome-mediated centriole amplification, as revealed by the specific expression of *MCIDAS*[8], *MYB*[24], and *DEUP1*[21] (Fig. 1c,d and Supplementary Figure 1). This subpopulation was characterized by the expression of known effectors of centriole synthesis, such as *PLK4*, *STIL*, *CEP152*, *SASS6*, but also of cell cycle regulators, such as *CDK1*, *CCNB1*, *CDC20*, *SGOL2* and *NEK2* (Fig. 1d, Supplementary Figure 1 and Supplementary Table 1). We

reasoned that uncharacterized cell cycle-related genes that are specific to this subpopulation could encode new components of the deuterosome-dependent centriole amplification pathway. A particularly interesting candidate in this category was *CDC20B* (Fig. 1d), which is related to the cell cycle regulators *CDC20* and *FZR1*[25] (Supplementary Figure 2a). First, the *CDC20B* gene is present in the vertebrate genomic locus that also contains the key MCC regulators *MCIDAS*[8] and *CCNO*[13]. Co-expression of *CDC20B*, *MCIDAS* and *CCNO* throughout HAEC differentiation was indeed observed in an independent RNA sequencing study, performed on a bulk population of HAECs (Supplementary Figure 2b). These results fit well with the observation that the promoter of human *CDC20B* was strongly activated by the MCIDAS partners E2F1 and E2F4 (Supplementary Figure 2c), as also shown in *Xenopus* by others[9] (Supplementary Figure 2d). Second, the *CDC20B* gene bears in its second intron the miR-449 microRNAs, which were shown to contribute to MCC differentiation[23, 26-30]. Finally, in *Xenopus* epidermal MCCs, *cdc20b* transcripts were specifically detected during the phase of centriole amplification (Supplementary Figure 2e-m). This first set of data pointed out the specific and conserved expression pattern of *CDC20B* in immature MCCs. In the rest of this study, we analyzed the putative role of CDC20B in deuterosome-mediated centriole multiplication.

Composition and organization of vertebrate deuterosomes

We first conducted a series of immunofluorescence analyses to gain a better understanding of deuterosome organization in mouse ependymal and *Xenopus* epidermal MCCs as models. In whole-mounts of mouse ependymal walls, mature deuterosomes revealed by DEUP1 staining appeared as circular structures around a lumen (Fig. 2a). We noticed that DEUP1 also stained fibers emanating from the core into the corona. Nascent centrioles revealed by the marker FOP were organized around the DEUP1-positive core ring. STED super-resolution

120 microscopy helped to better appreciate the regular organization of individual FOP-positive
121 procentrioles (Fig. 2b). Proximity labeling assays have revealed that when ectopically
122 expressed in centrosomes CCDC67/DEUP1 is found close to Pericentrin (PCNT) and γ-
123 tubulin, two main components of the pericentriolar material (PCM)[31]. Interestingly, we found
124 that PCNT was present in the deuterosome corona (Fig. 2a), and STED microscopy further
125 revealed that PCNT formed fibers around growing procentrioles (Fig. 2b). γ-tubulin staining
126 was detected in the DEUP1-positive deuterosome core, as well as in the corona (Fig. 2a).
127 STED microscopy indicated that PCNT and γ-tubulin stained distinct interwoven fibers in the
128 deuterosome corona. Next, we stained immature *Xenopus* epidermal MCCs with γ-Tubulin
129 and Centrin to reveal centriole amplification platforms. These platforms displayed irregular
130 shapes and sizes (Fig. 2c), in agreement with early electron microscopy studies[18]. Expression
131 of low amounts of GFP-Deup1 in MCCs induced by Multicilin confirmed that active
132 deuterosomes are embedded in γ-Tubulin-positive masses (Fig. 2d). Overall, this analysis is
133 consistent with early ultrastructural studies, as the deuterosome core and corona can be
134 distinguished by the presence of DEUP1 and PCNT, respectively. Moreover, γ-tubulin is a
135 conserved marker of centriole amplification platforms in vertebrate MCCs. By analogy to the
136 organization of the centrosome, we propose to coin the term perideuterosomal material
137 (PDM) to describe the corona, as this region may prove important for deuterosome function.
138
139 **CDC20B associates to vertebrate deuterosomes**
140 We then analyzed the subcellular localization of CDC20B protein in deuterosome-stage
141 mouse and *Xenopus* MCCs. In immature mouse tracheal MCCs, double immunofluorescence
142 revealed the association of CDC20B to DEUP1-positive deuterosomes (Fig. 3a). We noticed
143 that CDC20B tended to associate primarily to large DEUP1 foci. As deuterosomes grow as
144 they mature[21], this suggests that CDC20B may penetrate into the deuterosomal environment

at a late stage of the centriole multiplication process. The same observation was made when comparing CDC20B staining in the region of immature and mature deuterosomes of mouse ependymal MCCs (Fig. 3b). As double DEUP1/CDC20B staining could not be performed on these cells, we analyzed CDC20B distribution relative to FOP-positive procentrioles. In early deuterosome-stage MCCs, CDC20B was expressed at low levels and FOP staining was mostly concentrated in a large amorphous cloud (Fig. 3b). In such cells, no CDC20B staining was detected in association to FOP-positive procentrioles growing around deuterosomes. In contrast, in mature deuterosome-stage MCCs, CDC20B was enriched in the innermost part of the PDM, probably very close to the deuterosome core (Fig. 3b). Further evidence was provided with a custom-made polyclonal antibody (Supplementary Figure 3b,c) used to analyze Cdc20b protein distribution in *Xenopus* epidermal MCCs. Here also, Cdc20b was found associated to Deup1-positive deuterosomes actively engaged in centriole synthesis (Fig. 3c). We finally analyzed the distribution of CDC20B in mature MCCs. As previously reported, the CDC20B protein was detected near BBs[23], but also in cilia of fully differentiated human airway MCCs (Supplementary Figure 4a-c). This was confirmed by proximity ligation assays that revealed a tight association of CDC20B with Centrin2 and acetylated α-Tubulin, in BBs and cilia, respectively (Supplementary Figure 4d-f). Fluorescent immunostaining also revealed the presence of Cdc20b in the vicinity of BBs in *Xenopus* epidermal MCCs (Supplementary Figure 4g-i). In contrast, no cilia staining was observed in these cells. Altogether, our analyses revealed that in three distinct types of MCCs in two distant vertebrate species, CDC20B is tightly associated to mature deuterosomes. We next investigated whether it may control their function.

CDC20B is required for multiciliogenesis in vertebrates

For that purpose, *Cdc20b* was knocked down in mouse ependymal MCCs, through post-natal brain electroporation of three distinct shRNAs. One of them, sh274, which targets the junction between exons 3 and 4, and can therefore only interact with mature mRNA, was useful to rule out possible interference with the production of miR-449 molecules from the *Cdc20b* pre-mRNA (Supplementary Figure 5a). Five days after electroporation, all three shRNAs significantly reduced the expression of CDC20B in deuterosome-stage MCCs (Fig. 4c), but did not alter MCC identity as revealed by FOXJ1 expression (Fig. 4a,b,d). Centriole production by deuterosomes was analyzed by FOP/DEUP1 double staining nine days after electroporation. At this stage, control MCCs had nearly all released their centrioles and disassembled their deuterosomes (Fig. 4e,g). In sharp contrast, *Cdc20b* shRNAs caused a significant increase in the number of defective MCCs that displayed centrioles still engaged on deuterosomes (Fig. 4f,g). Fifteen days after electroporation, a majority of CDC20B-deficient MCCs still showed a severely reduced number of released centrioles, and consequently lacked cilia (Fig. 4h-k).

Cdc20b was also knocked down in *Xenopus* epidermal MCCs, through injection of two independent morpholino antisense oligonucleotides targeting either the ATG (Mo ATG), or the exon 1/intron 1 junction (Mo Spl) (Supplementary Figure 5b). The efficiency of Mo ATG was verified through fluorescence extinction of co-injected Cdc20b-Venus (Supplementary Figure 5c). RT-PCR confirmed that Mo Spl caused intron 1 retention (Supplementary Figure 5d), which was expected to introduce a premature stop codon, and to produce a Cdc20b protein lacking 96% of its amino-acids, likely to undergo unfolded protein response-mediated degradation. Thus, both morpholinos were expected to generate severe loss of Cdc20b function. Consistent with this interpretation, both morpholinos strongly reduced Cdc20b immunostaining in deuterosome-stage MCCs (Supplementary Figure 5e). We verified that neither morpholinos caused *p53* transcript up-regulation (Supplementary Figure 5f), a non-

194 specific response to morpholinos that is sometimes detected in zebrafish embryos[32].
195 Importantly, whole-mount *in situ* hybridization indicated that miR-449 expression was not
196 perturbed in the presence of either morpholino (Supplementary Figure 5g). We found that
197 *cdc20b* knockdown did not interfere with acquisition of the MCC fate (Supplementary Figure
198 6a-e), but severely impaired multiciliogenesis, as revealed by immunofluorescence and
199 electron microscopy (Fig. 5a-i). This defect stemmed from a dramatic reduction in the number
200 of centrioles, and poor docking at the plasma membrane (Fig. 5g-o and Supplementary Figure
201 6f-k). Importantly, centrioles and cilia were rescued in Mo Spl MCCs by co-injection of
202 *cdc20b*, *venus-cdc20b* or *cdc20b-venus* mRNAs (Fig. 5j-o and Supplementary Figure 6f-k). In
203 normal condition, *Xenopus* epidermal MCCs arise in the inner mesenchymal layer and
204 intercalate into the outer epithelial layer, while the process of centriole amplification is
205 underway[33]. To rule out secondary defects due to poor radial intercalation, we assessed the
206 consequences of *cdc20b* knockdown in MCCs induced in the outer layer by Multicilin
207 overexpression[8]. Like in natural MCCs, Cdc20b proved to be essential for the production of
208 centrioles and cilia in response to Multicilin activity (Supplementary Figure 7a-g). We also
209 noted that the apical actin network that normally surrounds BBs was disrupted in absence of
210 Cdc20b, although this defect could be secondary to the absence of centrioles (Supplementary
211 Figure 7d-g). Centrioles in Cdc20b morphant cells often formed clusters, suggesting that
212 disengagement from deuterosomes could have failed (Fig. 5l,m). To better assess this process,
213 we injected GFP-Deup1 in Multicilin-induced MCCs and stained centrioles with Centrin. In
214 mature control MCCs, deuterosomes were disassembled, centrioles were converted into BBs,
215 had docked and initiated cilium growth (Fig. 5p,s). In contrast, both morpholinos caused a
216 dramatic increase in the number of defective MCCs, which were devoid of cilia and displayed
217 centrioles still engaged on deuterosomes (Fig. 5q-u). Altogether our functional assays in
218 mouse and *Xenopus* indicate that CDC20B is required for centriole disengagement from

deuterosomes and subsequent ciliogenesis in MCCs. We next investigated the molecular mechanism of action of CDC20B underlying its role in centriole release.

Partners and effectors of CDC20B reveal its mechanism of action

In mitotic cells, centriole disengagement is necessary to license centriole duplication in the following cell cycle[34]. This process is known to depend on the coordinated activities of the mitotic kinase PLK1 and the protease Separase[35]. One proposed mechanism involves the phosphorylation of PCNT by PLK1, which induces its cleavage by Separase, thereby allowing centriole disengagement through disassembly of the PCM[36, 37]. Separase is known to be activated by the degradation of its inhibitor Securin, which is triggered by the Anaphase Promoting Complex (APC/C) upon binding to CDC20[25]. *PLK1*, *Separase* (*ESPL1*), *Securin* (*PTTG1*), *CDC20* and *PCNT* were all found to be expressed in human deuterosome-stage MCCs (Fig. 1d and Supplementary Figure 1). We have shown above that PCNT is present in the PDM and a recent study revealed the presence of CDC20 and the APC/C component APC3 in mouse ependymal MCCs at the stage of centriole disengagement[38]. Based on this large body of information, we hypothesized that centriole-deuterosome disengagement involves the coordinated activities of PLK1 and Separase, and that CDC20B would be involved in this scenario. *CDC20B* encodes a protein of about 519 amino-acids largely distributed across the vertebrate phylum[23]. In its C-terminal half, CDC20B contains seven well conserved WD40 repeats, predicted to form a β-propeller, showing 49% and 37% identity to CDC20 and FZR1 repeats, respectively (Supplementary Figure 2a). However, CDC20B lacks canonical APC/C binding domains (Supplementary Figure 2a). Using mass spectrometry on immunoprecipitated protein complexes from transfected HEK cells, we could identify multiple APC/C components interacting with CDC20 but not with CDC20B (Supplementary Table 2). We conclude that CDC20B is probably incapable of activating

APC/C. Interestingly, an unbiased interactome study reported association of CDC20B with PLK1[39]. Using reciprocal co-immunoprecipitation assays in HEK transfected cells, we confirmed that CDC20B and PLK1 could be found in the same complex (Fig. 6a and Supplementary Figure 8). This suggested that CDC20B could cooperate with PLK1 to trigger centriole disengagement. Consistent with this hypothesis, we found that PLK1 was enriched in the PDM of mature deuterosomes in mouse ependymal MCCs (Fig. 6b), in agreement with a recent report[38]. Another interesting partner of CDC20B identified in a second unbiased interactome study[40] was SPAG5 (Astrin), which was reported to control timely activation of Separase during the cell cycle[41, 42]. Using the same strategy as above, we could detect CDC20B and SPAG5 in the same complex (Fig. 6c and Supplementary Figure 8). As SPAG5 was found associated to DEUP1 in a proximity labeling assay[31], we assessed its localization in deuterosomes. Strikingly, SPAG5 was detectable in mature deuterosomes of mouse ependymal MCCs, with a clear enrichment in the deuterosome core (Fig. 6d). Finally, reciprocal co-immunoprecipitations revealed that CDC20B and DEUP1 were detected in the same complex when co-expressed in HEK cells (Fig. 6e and Supplementary Figure 8). Consistent with this result, we observed that RFP-Cdc20b was recruited around spherical Deup1-GFP structures positive for γ-Tubulin and Centrin in *Xenopus* epidermal MCCs (Supplementary Figure 7h-m). This series of experiments suggested that CDC20B could participate in the assembly of a protein complex in mature deuterosomes, required to coordinate the activities of PLK1 and Separase for centriole disengagement. As Separase is the last effector in this scenario, we tested whether over-expressing human Separase in *Xenopus cdc20b* morphant MCCs could rescue centriole disengagement. In support to our hypothesis, over-expression of wild-type, but not protease-dead Separase, efficiently rescued centriole disengagement and cilia formation in *cdc20b* morphant MCCs (Fig. 7a-g and Supplementary Figure 7n-s). Separase could also rescue multiciliogenesis in Multicilin-

induced MCCs injected with *cdc20b* Mos (Supplementary Figure 7t-z). We conclude that CDC20B is involved in Separase-mediated release of mature centrioles from deuterosomes in vertebrate MCCs (Fig. 7h).

Discussion

In this study, we report for the first time the essential and conserved role of CDC20B in vertebrate multiciliogenesis. Our data suggest that the presence of CDC20B in the perideuterosomal region is necessary to allow centriole disengagement. We note, however, that our data, which are based on partial knockdowns, remain compatible with an earlier function of CDC20B in promoting deuterosome assembly and/or activity. A total genetic knockout of *Cdc20b* should help to assess this possibility in mouse tracheal and ependymal MCCs. By analogy to mitosis, we propose that CDC20B is involved in Separase-dependent proteolysis at deuterosomes, allowing the release of mature centrioles and subsequent ciliogenesis. This view is consistent with a recent report showing that centriole disengagement in murine ependymal MCCs involves the activities of PLK1, a partner of CDC20B, and APC/C, the activator of Separase[38]. The central question arising from our work then becomes: how are CDC20B and Separase activities integrated? The simple scenario of a CDC20-like function of CDC20B is very unlikely as it does not appear to bind APC/C (Supplementary Table 2). CDC20 was detected in cultured murine ependymal MCCs during the phase of centriole disengagement[38], and FZR1 genetic ablation was reported to cause reduced production of centrioles and cilia in the same cells[43]. APC/C is therefore likely activated in maturing MCCs by its classical activators, CDC20 and/or FZR1, leading to Separase activation through degradation of its inhibitor Securin. In that context, we propose that additional factors linked directly or indirectly to CDC20B may contribute to activation of Separase. It was shown that SPAG5 inhibits or activates Separase depending on its status of

294 phosphorylation[41, 42]. As the phosphorylation status of SPAG5 was shown to be controlled by
295 PLK1[44], our data suggest that the CDC20B/PLK1/SPAG5 complex could control the timing
296 of Separase activation locally in deuterosomes. It is therefore possible that multiple modes of
297 activation of Separase may act in parallel to trigger the release of neo-synthesized centrioles
298 in maturing MCCs. Alternatively, different pathways may be used in distinct species, or in
299 distinct types of MCCs. An important question for future studies regards the identity of PLK1
300 and Separase substrates involved in centriole disengagement. Work on mitotic cells[36, 37] and
301 our own analysis suggest that PCNT may represent a prime target. Another potentially
302 relevant candidate could be DEUP1 itself as it is clear that deuterosomes are disassembled
303 after the release of centrioles. In that respect, it is interesting to note the presence of multiple
304 PLK1 consensus phosphorylation sites in human, mouse and *Xenopus* DEUP1.
305 In this study, we have introduced the notion of perideuterosomal material, in analogy to the
306 pericentriolar material. It is striking that the two main components of the PCM, PCNT and γ-
307 Tubulin, are also present in the PDM, which begs the question whether additional PCM
308 proteins may be present in the PDM. The PDM may constitute a platform to sustain
309 procentriole growth, through the concentration and delivery of elementary parts. It could also
310 play a mechanical role to hold in place the growing procentrioles. Future work should
311 evaluate deuterosome-mediated centriole synthesis in absence of major PDM components.
312 We found that beyond its association to deuterosomes during the phase of centriole
313 amplification, CDC20B was also associated to BBs and cilia in fully differentiated
314 mammalian MCCs. This dual localization is consistent with failed ciliogenesis upon CDC20B
315 knockdown in mouse ependymal MCCs. However, while we could detect Cdc20b near BBs
316 of mature MCCs in *Xenopus*, we found no evidence of its presence in cilia. Furthermore, cilia
317 were rescued by Separase overexpression in Cdc20b morphant MCCs. This suggests that
318 Cdc20b is not required for ciliogenesis in this species, although it could potentially contribute

to cilium structure and/or function. Thus, refined temporal and spatial control of CDC20B inhibition will be needed to study its function beyond centriole synthesis.

This and previous studies[23, 26-28] establish that the miR-449 cluster and its host gene *CDC20B* are commonly involved in multiciliogenesis. Consistent with its early expression, it was suggested that miR-449 controls cell cycle exit and entry into differentiation of MCCs[23, 27, 30]. This study reveals that CDC20B itself is involved in the production of centrioles, the first key step of the multiciliogenesis process. From that perspective, the nested organization of miR-449 and *CDC20B* in vertebrate genomes, which allows their coordinated expression, appears crucial for successful multiciliogenesis.

It is also noteworthy to point out the location of this gene in a genomic locus where congenital mutations in MCIDAS and CCNO were recently shown to cause a newly-recognized MCC-specific disease, called Reduced Generation of Multiple motile Cilia (RGMC). RGMC is characterized by severe chronic lung infections and increased risk of infertility[12, 13]. Its location in the same genetic locus as MCIDAS and CCNO makes CDC20B a putative candidate for RGMC. By extension, new deuterosome-stage specific genes uncovered by scRNA-seq in this study also represent potential candidates for additional RGMC mutations.

Previous works have established the involvement of the centriole duplication machinery active in S-phase of the cell cycle, during centriole multiplication of vertebrate post-mitotic MCCs[19-21]. Our study further reveals a striking analogy between centriole disengagement from deuterosomes in MCCs, and centriole disengagement that occurs during the M/G1 transition of the cell cycle (Fig. 7g). Thus, it appears that centriole production in MCCs recapitulates the key steps of the centriole duplication cycle[34]. However, the cell cycle machinery must adapt to the acentriolar deuterosome to massively produce centrioles. Such adaptation appears to involve physical and functional interactions between canonical cell

cycle molecules, such as CEP152 and PLK1, and recently evolved cell cycle-related deuterosomal molecules, such as DEUP1[21] and CDC20B. It remains to examine whether additional deuterosomal cell cycle-related molecules have emerged in the vertebrate phylum to sustain massive centriole production.

In conclusion, this work illustrates how coordination between ancestral and recently evolved cell cycle-related molecules can give rise to a new differentiation mechanism in vertebrates.

Methods

Subjects/human samples

Inferior turbinates were from patients who underwent surgical intervention for nasal obstruction or septoplasty (provided by L. Castillo, Nice University Hospital, France). The use of human tissues was authorized by the bioethical law 94-654 of the French Public Health Code and written consent from the patients.

Single-cell RNA sequencing of Human Airway Epithelial Cells (HAECs)

HAECs cultures were derived from nasal mucosa of inferior turbinates. After excision, nasal inferior turbinates were immediately immersed in Ca2+/Mg2+-free HBSS supplemented with 25 mM HEPES, 200 U/mL penicillin, 200 µg/mL streptomycin, 50 µg/mL gentamicin sulfate, and 2.5 µg/ml amphotericin B (all reagents from Gibco). After repeated washes with cold supplemented HBSS, tissues were digested with 0.1% Protease XIV from *Streptomyces Griseus* (Sigma) overnight at 4°C. After incubation, fetal calf serum (FCS) was added to a final concentration of 10%, and nasal epithelial cells were detached from the stroma by gentle agitation. Cell suspensions were further dissociated by trituration through a 21G-needle and then centrifuged at 150g for 5 min. The pellet was resuspended in supplemented HBSS containing 10% FCS and centrifuged again. The second cell pellet was then suspended in

Dulbecco's Modified Eagle's Medium (DMEM, Gibco) containing 10% FCS and cells were plated (20 000 cells per cm²) on 75 cm²-flasks coated with rat-tail collagen I (Sigma-Aldrich). Cells were incubated in a humidified atmosphere of 5% CO2 at 37°C. Culture medium was replaced with Bronchial Epithelium Basal Medium (BEBM, Lonza) supplemented with BEGM SingleQuot Kit Supplements (Lonza) on the day after and was then changed every other day. After 4 to 5 days of culture, after reaching about 70% confluence, cells were detached with trypsin-EDTA 0.05% (Gibco) for 5 min and seeded on Transwell® permeable supports (6.5 mm diameter; 0.4 µm pore size; Corning), in BEGM medium, with a density of 30 000 cells per Transwell®. Once the cells have reached confluence (typically after 5 days), they were induced to differentiate at the air-liquid interface by removing medium at the apical side of the Transwell®, and by replacing medium at the basal side with DMEM:BEBM (1:1) supplemented with BEGM SingleQuot Kit Supplements. Culture medium was changed every other day. Single-cell analysis was performed after 14 days of culture at the air-liquid interface, which corresponds to the maximum centriole multiplication stage. To obtain a single-cell suspension, cells were incubated with 0.1% protease type XIV from *Streptomyces griseus* in supplemented HBSS for 4 hours at 4°C degrees. Cells were gently detached from Transwells® by pipetting and then transferred to a microtube. 50 units of DNase I (EN0523 Thermo Fisher Scientific) per 250 µL were directly added and cells were further incubated at room temperature for 10 min. Cells were centrifuged (150g for 5 min) and resuspended in 500 µL supplemented HBSS containing 10% FCS, centrifuged again (150g for 5 min) and resuspended in 500 µL HBSS before being mechanically dissociated through a 26G syringe (4 times). Finally, cell suspensions were filtered through a Scienceware® Flowmi™ Cell Strainer (40µm porosity), centrifuged (150g for 5 min) and resuspended in 500 µL of cold HBSS. Cell concentration measurements were performed with Scepter™ 2.0 Cell Counter (Millipore) and Countess™ automated cell counter (ThermoFisher Scientific). Cell viability

was checked with Countess™ automated cell counter (ThermoFisher Scientific). All steps except the DNAse I incubation were performed on ice. For the cell capture by the 10X genomics device, the cell concentration was adjusted to 300 cells/µl in HBSS aiming to capture 1500 cells. We then followed the manufacturer's protocol (Chromium™ Single Cell 3' Reagent Kit, v2 Chemistry) to obtain single cell 3' libraries for Illumina sequencing. Libraries were sequenced with a NextSeq 500/550 High Output v2 kit (75 cycles) that allows up to *91* cycles of paired-end sequencing: the forward read had a length of 26 bases that included the cell barcode and the UMI; the reverse read had a length of 57 bases that contained the cDNA insert. CellRanger Single-Cell Software Suite v1.3 was used to perform sample demultiplexing, barcode processing and single-cell 3′ gene counting using standards default parameters and human build hg19. Additional analyses were performed using R. Pseudotemporal ordering of single cells was performed with the last release of the Monocle package [45]. Cell cycle scores were calculated by summing the normalized intensities of genes belonging to phase-specific gene sets then centered and scaled by phase. Gene sets for each phase were curated from previously described sets of genes [46] (Table S2). Data was submitted to the GEO portal under series reference GSE103518. Data shown in Figure 1 is representative of 4 independent experiments performed on distinct primary cultures.

RNA sequencing of HAECs

For Figure S3A, three independent HAEC cultures (HAEC1, HAEC2, HAEC3) were triggered to differentiate in air-liquid interface (ALI) cultures for 2 days (ALI day 2, undifferentiated), ALI day 14 (first cilia) or ALI day 28 (well ciliated). RNA was extracted with the miRNeasy mini kit (Qiagen) following manufacturer's instructions. mRNA-seq was performed from 2 µg of RNA that was first subjected to mRNA selection with Dynabeads® mRNA Purification Kit (Invitrogen). mRNA was fragmented 10 min at 95°C in RNAseIII

419 buffer (Invitrogen) then adapter-ligated, reverse transcribed and amplified (6 cycles) with the
420 reagents from the NEBNext Small RNA Library Prep Set for SOLiD. Small RNA-seq was
421 performed from 500 ng RNA with the NEBNext Small RNA Library Prep Set for SOLiD (12
422 PCR cycles) according to manufacturer's instructions. Both types of amplified libraries were
423 purified on Purelink PCR micro kit (Invitrogen), then subjected to additional PCR rounds (8
424 cycles for RNA-seq and 4 cycles for small RNA-seq) with primers from the 5500 W
425 Conversion Primers Kit (Life Technologies). After Agencourt® AMPure® XP beads
426 purification (Beckman Coulter), libraries were size-selected from 150 nt to 250 nt (for RNA-
427 seq) and 105 nt to 130 nt (for small RNA-seq) with the LabChip XT DNA 300 Assay Kit
428 (Caliper Lifesciences), and finally quantified with the Bioanalyzer High Sensitivity DNA Kit
429 (Agilent). Libraries were sequenced on SOLiD 5500XL (Life Technologies) with single-end
430 50b reads. SOLiD data were analyzed with lifescope v2.5.1, using the small RNA pipeline for
431 miRNA libraries and whole transcriptome pipeline for RNA-seq libraries with default
432 parameters. Annotation files used for production of raw count tables correspond to Refseq
433 Gene model v20130707 for mRNAs and miRBase v18 for small RNAs. Data generated from
434 RNA sequencing were then analyzed with Bioconductor (http://www.bioconductor.org)
435 package DESeq and size-factor normalization was applied to the count tables. Heatmaps were
436 generated with GenePattern using the "Hierarchical Clustering" Module, applying median
437 row centering and Euclidian distance.
438
439 Re-analysis of *Xenopus* E2F4 Chip-seq and RNA-seq
440 RNA-seq (samples GSM1434783 to GSM1434788) and ChIP-seq (samples GSM1434789 to
441 GSM1434792) data were downloaded from GSE59309. Reads from RNA-seq were aligned to
442 the *Xenopus laevis* genome release 7.1 using TopHat2[47] with default parameters.
443 Quantification of genes was then performed using HTSeq-count[48] release 0.6.1 with "-m

intersection-nonempty" option. Normalization and statistical analysis were performed using Bioconductor package DESeq2[49]. Differential expression analysis was done between Multicilin-hGR alone versus Multicilin-hGR in the presence of E2f4ΔCT. Reads from ChIP-seq were mapped to the *Xenopus laevis* genome release 7.1 using Bowtie2[50]. Peaks were called and annotated according to their positions on known exons with HOMER[51]. Peak enrichments of E2F4 binding site in the promoters of centriole genes and cell cycle genes[9] were estimated in presence or absence of Multicilin and a ratio of E2F4 binding (Multicilin vs no Multicilin) was calculated.

Promoter reporter studies

The human *CDC20B* promoter was cloned into the pGL3 Firefly Luciferase reporter vector (Promega) with SacI and NheI cloning sites. The promoter sequenced ranged from -1073 to +104 relative to the transcription start site. 37.5 ng of pGL3 plasmid were applied per well. pCMV6-Neg, pCMV6-E2F1 (NM_005225) and pCMV6-E2F4 (NM_001950) constructs were from Origene. 37.5 ng of each plasmid was applied per well. 25 ng per well of pRL-CMV (Promega) was applied in the transfection mix for transfection normalization (Renilla luciferase). HEK 293T cells were seeded at 20 000 cells per well on 96-well plates. The following day, cells were transfected with the indicated plasmids (100 ng of total DNA) with lipofectamine 3000 (Invitrogen). After 24 hours, cells were processed with the DualGlo kit (Promega) and luciferase activity was recorded on a plate reader.

Proximity ligation Assays

Fully differentiated HAECs were dissociated by incubation with 0.1% protease type XIV from *Streptomyces griseus* (Sigma-Aldrich) in HBSS (Hanks' balanced salts) for 4 hours at 4°C. Cells were gently detached from the Transwells® by pipetting and then transferred to a

469 microtube. Cells were then cytocentrifuged at 300 rpm for 8 min onto SuperFrostPlus slides
470 using a Shandon Cytospin 3 cytocentrifuge. Slides were fixed for 10 min in methanol at -
471 20°C for Centrin2 and ZO1 assays, and for 10 min in 4% paraformaldehyde at room
472 temperature and then permeabilized with 0.5% Triton X-100 in PBS for 10 min for
473 Acetylated-α-tubulin assays. Cells were blocked with 3% BSA in PBS for 30 min. The
474 incubation with primary antibodies was carried out at room temperature for 2 h. Then, mouse
475 and rabbit secondary antibodies from the Duolink® Red kit (Sigma-Aldrich) were applied and
476 slides were processed according to manufacturer's instructions. Images were acquired using
477 the Olympus Fv10i confocal imaging systems with 60X oil immersion objective and Alexa
478 647 detection parameters.
479
480 Animals
481 All experiments were performed following the Directive 2010/63/EU of the European
482 parliament and of the council of 22 September 2010 on the protection of animals used for
483 scientific purposes. Experiments on *Xenopus laevis* and mouse were approved by the
484 'Direction départementale de la Protection des Populations, Pôle Alimentation, Santé
485 Animale, Environnement, des Bouches du Rhône' (agreement number F 13 055 21). Mouse
486 experiments were approved by the French ethical committee n°14 (permission number: 62-
487 12112012). Timed pregnant CD1 mice were used (Charles Rivers, Lyon, France).
488
489 Immunostaining on mouse ependyma
490 Dissected brains were subjected to 12 min fixation in 4% paraformaldehyde, 0.1% Triton X-
491 100, blocked 1 hour in PBS, 3% BSA, incubated overnight with primary antibodies diluted in
492 PBS, 3% BSA, and incubated 1 h with secondary antibodies at room temperature. Ependyma
493 were dissected further and mounted with Mowiol before imaging using an SP8 confocal

microscope (Leica microsystems) equipped with a 63x oil objective. The same protocol was used to prepare samples for super-resolution acquisition. Pictures were acquired with a TCS SP8 STED 3X microscope equipped with an HC PL APO 93X/1.30 GLYC motCORR™ objective (Leica microsystems). Pericentrin was revealed using Alexa 514 (detection 535-564nm, depletion 660nm), γ-tubulin was revealed using Alexa 568 (detection 582-667nm, depletion 775), and FOP was revealed using Alexa 488 (detection 498-531nm, depletion 592nm). Pictures were deconvoluted using Huygens software. Maximum intensity projection of 3 deconvoluted pictures is presented in Figure 4G. Primary antibodies: rabbit anti-CDC20B (1:500; Proteintech, 133376-1-AP), mouse IgG anti-PLK1 (1:500; Thermo Fisher, 33-1700), rabbit anti-Pericentrin (1:500, Abcam, ab4448), mouse IgG1 anti-FoxJ1 (1:1000; eBioscience, 14-9965), rabbit anti-Deup1 (1:1000; kindly provided by Dr Xueliang Zhu), rabbit anti-Deup1 (1:250; Proteintech, 24579-1-AP), mIgG1 anti-γ-Tubulin (clone GTU88) (1:250; Abcam, Ab 11316), rabbit anti-ZO1 (1:600; Thermo Fisher Scientific, 61-7300), rabbit anti-Spag5 (1:500; Proteintech, 14726-1-AP), mouse IgG1 anti-ZO1 (1:600; Invitrogen, 33-9100), mouse IgG2b anti-FGFR1OP (FOP) (1:2000; Abnova, H00011116-M01), mouse IgG1 anti-α-tubulin (1:500; Sigma-Aldrich, T9026). Secondary antibodies: Alexa Fluor 488 goat anti-rabbit (1:800; Thermo Fisher Scientific, A-11034), Alexa Fluor 647 goat anti-rabbit (1:800; Thermo Fisher Scientific, A-21244), Alexa Fluor 514 goat anti-rabbit (1:800; Thermo Fisher Scientific, A-31558), Alexa Fluor 488 goat anti-mouse IgG2b (1:800; Thermo Fisher Scientific, A-21141), Alexa Fluor 568 goat anti-mouse IgG2b (1:800; Thermo Fisher Scientific, A-21144), Alexa Fluor 488 goat anti-mouse IgG2a (1:800; Thermo Fisher Scientific, A-21131), Alexa Fluor 568 goat anti-mouse IgG1 (1:800; Thermo Fisher Scientific, A-21134), Alexa Fluor 647 goat anti-mouse IgG1 (1:800; Thermo Fisher Scientific, A-21240).

519 Mouse constructs

520 Expression constructs containing shRNA targeting specific sequences in the CDC20B coding
521 sequence under the control of the U6 promoter were obtained from Sigma-Aldrich (ref.
522 TRCN0000088273 (sh273), TRCN0000088274 (sh274), TRCN0000088277 (sh277)). PCX-
523 mcs2-GFP vector (Control GFP) kindly provided by Xavier Morin (ENS, Paris, France), and
524 U6 vector containing a validated shRNA targeting a specific sequence in the NeuroD1 coding
525 sequence[52] (Control sh, ref. TRCN0000081777, Sigma-Aldrich) were used as controls for
526 electroporation experiments.

527

528 Postnatal mouse brain electroporation

529 The detailed protocol for postnatal mouse brain electroporation established by Boutin and
530 colleagues[53] was used with minor modifications. Briefly, P1 pups were anesthetized by
531 hypothermia. A glass micropipette was inserted into the lateral ventricle, and 2 µl of plasmid
532 solution (concentration 3µg/µl) was injected by expiratory pressure using an aspirator tube
533 assembly (Drummond). Successfully injected animals were subjected to five 95V electrical
534 pulses (50 ms, separated by 950 ms intervals) using the CUY21 edit device (Nepagene,
535 Chiba, Japan), and 10 mm tweezer electrodes (CUY650P10, Nepagene) coated with
536 conductive gel (Signagel, Parker laboratories). Electroporated animals were reanimated in a
537 37°C incubator before returning to the mother.

538

539 Statistical analyses of mouse experiments

540 Analysis of CDC20B signal intensity in deuterosomes (graph in Fig. 3b). For each
541 category, >25 cells from two different animals were analyzed. Deuterosome regions were
542 delineated based on FOP staining and the intensity of CDC20B fluorescent immunostaining

543 was recorded using ImageJ software, and expressed as arbitrary units. Unpaired t test vs
544 immature: p=0,0005 (intermediate,***); p<0,0001 (Mature, ****).
545 Analysis of *Cdc20b* shRNAs efficiency (Fig. 4c): For each cell at the deuterosomal stage, the
546 intensity of CDC20B fluorescent immunostaining was recorded using ImageJ software and
547 expressed as arbitrary units. Data are mean ± sem. Two independent experiments were
548 analyzed. A minimum of 35 cells per condition was analyzed. n= 3, 4, 5 and 5 animals for sh
549 control, sh273, sh274 and sh277, respectively. Unpaired t test vs sh control: p<0.0001 (sh273,
550 sh274 and sh277 ****).
551 Analysis of the number of FOXJ1 positive cells at 5dpe (Fig. 4d): Unpaired t test vs sh
552 control: 0.3961 (sh273, ns), 0.1265 (sh274, ns), 0.3250 (sh277, ns).
553 Analysis of the number of cells with non-disengaged centrioles at 9dpe (Fig. 4g): 15-20 fields
554 were analyzed per condition. n= 4, 4, 3, and 4 animals for sh control, sh273, sh274 and sh277,
555 respectively, from 2 independent experiments. Unpaired t test vs sh control: p<0.0001 (sh273,
556 sh274, sh277 ****).
557 Analysis of the number of centrioles per cell at 15dpe (Fig. 4j): >100 cells were analyzed per
558 condition. n= 3, 3, 3, and 3 animals for sh control, sh273, sh274 and sh277, respectively, from
559 2 independent experiments. Unpaired t test vs sh control: p<0.0001 (sh273, sh274, sh277
560 ****).
561 Analysis of ependymal cell categories at 15dpe (Fig. 4k): Data are mean ± sem from three
562 independent experiments. More than 500 cells were analyzed for each condition. n= 4, 4, 3,
563 and 3 animals for sh control, sh273, sh274 and sh277, respectively. Unpaired t test vs sh
564 control: p= 0.0004 (sh273, ***), 0.0001 (sh274, ****), 0.0038 (sh277, **).
565
566 Mouse tracheal epithelial cells (MTECs)

MTECs cell cultures were established from the tracheas of 12 weeks-old mice. After dissection, tracheas were placed in cold DMEM:F-12 medium (1:1) supplemented with 15 mM HEPES, 100 U/mL penicillin, 100 µg/mL streptomycin, 50 µg/mL gentamicin sulfate, and 2.5 µg/ml amphotericin B. Each trachea was processed under a binocular microscope to remove as much conjunctive tissue as possible with small forceps and was opened longitudinally with small dissecting scissors. Tracheas were then placed in supplemented DMEM:F-12 containing 0.15% protease XIV from *Streptomyces Griseus*. After overnight incubation at 4°C, FCS was added to a final concentration of 10%, and tracheal epithelial cells were detached by gentle agitation. Cells were centrifuged at 400g for 10 min and resuspended in supplemented DMEM:F-12 containing 10% FCS. Cells were plated on regular cell culture plates and maintained in a humidified atmosphere of 5% CO2 at 37°C for 4 hours to allow attachment of putative contaminating fibroblast. Medium containing cells in suspension was further centrifuged at 400g for 5 min and cells were resuspended in supplemented DMEM:F-12 containing BEGM Singlequots kit supplements and 5% FCS. Cells were plated on rat tail collagen I-coated Transwell®. Typically, 5 tracheas resulted in 12 Transwells®. Medium was changed every other day. Air-liquid interface culture was conducted once transepithelial electrical resistance had reached a minimum of 1000 ohm/cm2 (measured with EVOM2, World Precision Instruments).

Air-liquid interface culture was obtained by removing medium at the apical side of the Transwell®, and by replacing medium at the basal side with supplemented DMEM:F-12 containing 2% Ultroser-G™ (Pall Corporation). 10 µM DAPT (N-[N-(3,5-difluorophenacetyl)-L- alanyl]-S-phenylglycine t-butyl ester) (Sigma) was added one day after setting-up the air-liquid interface.

Immunostaining on HAECs and MTECs

Three days after setting-up the air-liquid interface, MTECs on Transwell membranes were pre-extracted with 0.5% Triton X-100 in PBS for 3 min, and then fixed with 4% paraformaldehyde in PBS for 15 min at room temperature. HAECs were treated 21 days after setting-up the air-liquid interface. They were fixed directly on Transwells® with 100% cold methanol for 10 min at -20°C (for CDC20B and Centrin2 co-staining, Supplementary Figure 4a,b) or with 4% paraformaldehyde in PBS for 15 min at room temperature (for CDC20B single staining, Supplementary Figure 4c). All cells were then permeabilized with 0.5% Triton X-100 in PBS for 5 min and blocked with 3% BSA in PBS for 30 min. The incubation with primary and secondary antibodies was carried out at room temperature for 2 h and 1 h, respectively. Nuclei were stained with 4,6-diamidino-2-phenylindole (DAPI). Transwell® membranes were cut with a razor blade and mounted with ProLong Gold medium (Thermofisher). Primary antibodies: rabbit anti-CDC20B (1:500; Proteintech, 133376-1-AP), rabbit anti-DEUP1 (1:500; Proteintech, 24579-1-AP), anti-Centrin2 (Clone 20H5, 1:500; Millipore, 04-1624). Secondary antibodies: Alexa Fluor 488 goat anti-rabbit (1:1000; Thermo Fisher Scientific, A-11034), Alexa Fluor 647 goat anti-mouse (1:1000; Thermo Fisher Scientific, A-21235). For co-staining of CDC20B and DEUP1, CDC20B primary antibody was directly coupled to CF^{TM} 633 with the Mix-n-Stain^{TM} kit (Sigma-Aldrich) according to the manufacturer's instruction. Coupled primary antibody was applied after secondary antibodies had been extensively washed and after a 30 min blocking stage in 3% normal rabbit serum in PBS.

Western blot and immunofluorescence on transfected cells

Cos1 or Hela cells cells were grown in DMEM supplemented with 10% heat inactivated FCS and transfected with Fugene HD (Roche Applied Science) according to manufacturer's protocol. Transfected or control cells were washed in PBS and lysed in 50 mM Tris-HCl pH

7.5, 150 mM NaCl, 1mM EDTA, containing 1% NP-40 and 0.25% sodium deoxycholate (modified RIPA) plus a Complete Protease Inhibitor Cocktail (Roche Applied Science) on ice. Cell extracts separated on polyacrylamide gels were transfered onto Optitran membrane (Whatman) followed by incubation with rabbit anti-mouse CDC20B (1:500, Proteintech, 24579-1-AP) or homemade rabbit anti-*Xenopus* Cdc20b (1:300) antibody and horseradish peroxidase conjugated secondary antibody (Jackson Immunoresearch Laboratories, 711-035-152 and 715-035-150). Signal obtained from enhanced chemiluminescence (Western Lightning ECL Pro, Perkin Elmer) was detected with MyECL Imager (Thermo Fisher Scientific).

For immunofluorescence staining, transfected cells were grown on glass coverslips and fixed for 6 min in methanol at -20°C. Cells were washed in PBS, blocked in PBS, 3% BSA and stained with rabbit anti-*Xenopus* Cdc20b (1:300) or rabbit anti-CFTR (1:200, Santa-Cruz Biotechnology, 10747) as a negative control, in blocking buffer. After washings in PBS 0.1% Tween-20, cells were incubated with Alexa fluor 488 donkey anti-rabbit antibody (Thermo Fisher Scientific, R37118), washed, and DNA was stained with 250 ng/ml DAPI. Coverslip were then rinsed and mounted in Prolong Gold antifade reagent (ThermoFisher Scientific) and confocal images were acquired by capturing Z-series with 0.3 µm step size on a Zeiss LSM 510 laser scanning confocal microscope.

Co-immunoprecipitation studies

Asynchronous HEK cells were rinsed on ice with chilled Ca++ and Mg++ free Dulbecco's PBS (DPBS, Invitrogen), harvested using a cell scraper and lysed on ice for 5 min in lysis buffer (0.025M Tris, 0.15M NaCl, 0.001M EDTA, 1% NP-40, 5% glycerol; pH 7.4) supplemented with EDTA and Halt™ Protease and Phosphatase Inhibitor Cocktail (Pierce, Thermofisher). Lysates were clarified (12000g, 4°C, 10 min) and the protein concentrations

642 were determined using the Bradford assay (Bio-Rad). Immunoprecipitations were performed
643 with the Pierce co-immunoprecipitation kit (Pierce, Thermofisher) according to the
644 manufacturer's instructions. For each immunoprecipitation, 1-1.5 mg of total lysate was
645 precleared on a control column, then incubated on columns coupled with 20 µg of anti-GFP
646 or anti-c-myc-antibody (clone 9E10). Incubation was performed overnight at 4°C. Columns
647 were washed and eluted with 50 µL elution buffer. Samples were denatured at 70°C for 10
648 min with Bolt™ LDS Sample Buffer and Bolt reducing agent, then separated on 4-12%
649 gradient Bolt precast gels (Thermofisher), transferred onto nitrocellulose (Millipore), and
650 subjected to immunoblot analysis using either anti-CDC20B (ProteinTech, 133376-1-AP) or
651 anti-c-myc antibody (clone 9E10). In Figure 6, note that the high level of expression of myc-
652 PLK1 (**a**) and myc-SPAG5 (**b**) drained out locally the ECL reagent at the peak of the protein.
653 The resulting double bands correspond in fact to unique ones. Human SPAG5, subcloned into
654 pCMV6-MT, was from OriGene. Human DEUP1 and PLK1 were cloned into pCS2-MT
655 vector (Addgene). Human CDC20B was cloned into pEGFP-C1, pEGFP-N1 (Clontech) for
656 the GFP fusion protein and pIRES-EYFP (Addgene) for the untagged protein.
657
658 In-Gel digestion, NanoHPLC, and Q-exactive*plus* analysis
659 For mass spectrometry analysis, protein spots were manually excised from the gel and
660 destained with 100 µL of H2O/ACN (1/1). After 10 min vortexing, liquid was discarded, and
661 the procedure was repeated 2 times. They were rinsed with acetonitrile and dried under
662 vacuum. Extracts were reduced with 50 µL of 10 mM dithiothreitol for 30 min at 56 °C, then
663 alkylated with 15 µL of 55 mM iodoacetamide for 15 min at room temperature in the dark.
664 They were washed successively by: i) 100 µL of H2O/ACN (1/1) (2 times) and ii) 100 µL of
665 acetonitrile. Gel pieces were rehydrated in 60 µL of 50 mM NH_4HCO_3 containing 10 ng/µL
666 of trypsin (modified porcine trypsin, sequence grade, Promega) incubated for one hour at 4°C.

After the removal of trypsin, samples were incubated overnight at 37°C. Tryptic peptides were extracted with: i) 60 µL of 1% FA (formic acid) in water (10 min at RT), ii) 60 µL acetonitrile (10 min at RT). Extracts were pooled, concentrated under vacuum, resuspended in 15 µL of aqueous 0.1% formic acid for NanoHPLC separation.

Separation was carried out using a nanoHPLC (Ultimate *3000,* Thermo Fisher Scientific). After concentration on a µ-Precolumn Cartridge Acclaim PepMap 100 C_{18} (i.d. 5 mm, 5 µm, 100 Å, Thermo Fisher Scientific) at a flow rate of 10 µL/min, using a solution of H_2O/ACN/FA 98%/2%/0.1%, a second peptide separation was performed on a 75 µm i.d. x 250 mm (3 µm, 100 Å) Acclaim PepMap 100 C_{18} column (Thermo Fisher Scientific) at a flow rate of 300 nL/min. Solvent systems were: (A) 100% water, 0.1% FA, (B) 100% acetonitrile, 0.08% FA. The following gradient was used t = 0min 6% B; t = 3 min 6%B; t = 119min, 45% B; t = 120 min, 90% B; t = 130 min 90% B (temperature at 35°C).

NanoHPLC was coupled via a nanoelectrospray ionization source to the Hybrid Quadrupole-Orbitrap High Resolution Mass Spectrometer (Thermo Fisher Scientific). MS spectra were acquired at a resolution of 70 000 (200 m/z) in a mass range of 300−2000 m/z with an AGC target 3e6 value of and a maximum injection time of 100ms. The 10 most intense precursor ions were selected and isolated with a window of 2m/z and fragmented by HCD (Higher energy C-Trap Dissociation) with normalized collision energy (NCE) of 27. MS/MS spectra were acquired in the ion trap with an AGC target 2e5 value, the resolution was set at 17 500 at 200 m/z combined with an injection time of 100 ms.

Data were reprocessed using Proteome Discoverer 2.1 equipped with Sequest HT. Files were searched against the Swissprot Homo sapiens FASTA database (update of February 2016). A mass accuracy of ± 10 ppm was used to precursor ions and 0.02 Da for product ions. Enzyme specificity was fixed to trypsin, allowing at most two miscleavages. Because of the previous chemical modifications, carbamidomethylation of cysteines was set as a fixed modification

and only oxydation of methionine was considered as a dynamic modification. Reverse decoy databases were included for all searches to estimate false discovery rates, and filtered using the Percolator algorithm at a 1% FDR.

Xenopus embryo injections, plasmids, RNAs, and morpholinos

Eggs obtained from NASCO females were fertilized *in vitro*, dejellied and cultured using standard protocols[54]. All injections were done at the 8-cell stage in one animal-ventral blastomere (presumptive epidermis), except for electron microscopy analysis for which both sides of the embryo was injected, and for RT-PCR analysis for which 2-cell embryos were injected.

cdc20b riboprobe was generated from *Xenopus laevis* cDNA. Full-length sequence was subcloned in pGEM™-T Easy Vector Systems (Promega). For sense probe it was linearized by SpeI and transcribed by T7. For antisense probe it was linearized by ApaI and transcribed by Sp6 RNA polymerase. Synthetic capped mRNAs were produced with the Ambion mMESSAGE mMACHINE Kit. pCS105/GFP-CAAX was linearized with AseI and mRNA was synthesized with Sp6 polymerase. pCS2-mRFP and pCS2-GFP-gpi were linearized with NotI and mRNA was synthesized with Sp6 polymerase. pCS-Centrin4-YFP (a gift from Reinhard Köster, Technische Universität Braunschweig, Germany) was linearized with NotI and mRNA was synthesized with Sp6 polymerase. pCS2-GFP-Deup1 and pCS2-Multicilin(MCI)-hGR were kindly provided by Chris Kintner; both plasmids were linearized with ApaI, and mRNAs were synthesized with Sp6 polymerase. Embryos injected with *MCI-hGR* mRNA were cultured in Dexamethasone 20µM in MBS 0,1X from st11 until fixation. pCS2-Separase wild-type and phosphomutant 2/4 (protease dead, PD) were provided by Marc Kirchner and Olaf Stemann, respectively; plasmids were linearized with NotI and mRNAs were synthesized with Sp6 polymerase. *Venus-cdc20b*, *cdc20b-Venus* and *cdc20b* were

717 generated by GATEWAY™ Cloning Technology (GIBCO BRL) from *Xenopus laevis cdc20b*
718 cDNA. *cdc20b* was also subcloned in pCS2-RFP to make *RFP-cdc20b* and *cdc20b-RFP*
719 fusions. All *cdc20b* constructs were linearized with NotI and mRNAs were synthesized with
720 Sp6 polymerase. Quantities of mRNA injected: 500pg for *GFP-CAAX*, *RFP*, *GFP-gpi,*
721 *Separase* and *Separase(PD);* 25 to 500pg for *GFP-Deup1*; 40 to 500pg for *MCI-hGR*; 1ng
722 for *Venus-cdc20b*, *cdc20b-Venus*, *cdc20b*, and *cdc20b-RFP*; 500pg to 1ng for *RFP-cdc20b.*
723 Two independent morpholino antisense oligonucleotides were designed against *cdc20b*
724 (GeneTools, LLC). *cdc20b* ATG Mo: 5'-aaatcttctctaacttccagtccat-3', *cdc20b* Spl Mo 5'-
725 acacatggcacaacgtacccacatc-3'. 20ng of MOs was injected per blastomere or 10ng of each Mo
726 for co-injection.
727
728 PCR and Quantitative RT-qPCR
729 *Xenopus* embryos were snap frozen at different stages and stored at -80°C. Total RNAs were
730 purified with a Qiagen RNeasy kit (Qiagen). Primers were designed using Primer-BLAST
731 Software. PCR reactions were carried out using GoTaq® G2 Flexi DNA Polymerase
732 (Promega). RT reactions were carried out using iScript™ Reverse Transcription Supermix for
733 RT-qPCR (BIO-RAD). qPCR reactions were carried out using SYBRGreen on a CFX Biorad
734 qPCR cycler. To check *cdc20b* temporal expression by qPCR we directed primers to exons
735 9/10 junction (Forward: 5'-ggctatgaattggtgcccg-3') and exons 10/11 junction (Reverse: 5'-
736 gcagggagcagatctggg-3') to avoid amplification from genomic DNA. The relative expression
737 of *cdc20b* was normalized to the expression of the housekeeping gene *ornithine*
738 *decarboxylase* (*ODC*) for which primers were as follows: forward: 5'-
739 gccattgtgaagactctctccattc-3': reverse: 5'-ttcgggtgattccttgccac-3'.

To check the efficiency of Mo SPL, expected to cause retention of intron1 in the mature mRNA of *cdc20b* we directed forward (5'-cctcccgagagttagagga-3') and reverse (5'-gcatgttgtactttctgctcca-3') primers in exon1 and exon2, respectively.

To check the expression of *p53* in morphants by qPCR, primers were as follows: forward: 5'-cgcagccgctatgagatgatt-3'; reverse: 5'-cacttgcggcacttaatggt-3'. The relative expression of p53 was normalized to Histone4 expression (H4) for which primers were as follows: forward: 5'-ggtgatgccctggatgttgt-3'; reverse: 5'-ggcaaaggaggaaaaggactg-3'.

Immunostainining on *Xenopus* embryos

Embryos were fixed in 4% paraformaldehyde (PFA) overnight at 4°C and stored in 100% methanol at -20°C. Embryos were rehydrated in PBT and washed in MABX (Maleic Acid Buffer + Triton X100 0,1% v/v). Next, embryos were incubated in Blocking Reagent (Roche) 2% BR + 15% Serum + MABX with respective primary and secondary antibodies. The anti-*Xenopus laevis* CDC20B antibody was obtained by rabbit immunization with the peptide SPDQRRIFSAAANGT (amino acids 495–509) conjugated to keyhole limpet hemocyanin, followed by affinity purification (Eurogentec). For immunofluorescence, embryos were fixed at RT in PFA 4% in PBS, and incubated in the CDC20B antibody diluted 1/150 in BSA 3% in PBS. For all experiments secondary antibodies conjugated with Alexa were used. GFP-CAAX in Supplementary Figure 5g was revealed using a rabbit anti-GFP antibody together with a secondary antibody coupled to Alkaline Phosphatase (AP), which was revealed as follows: embryos incubated with the AP-conjugated antibody were washed twice in alkaline phosphatase buffer (PAB) (NaCl 0.1M, Tris HCl pH 9.5 0.1M, MgCl2 0.05M, Tween 0.1%), 10 minutes each. Next, embryos were incubated in PAB with INT/BCIP substrate (Roche, REF:11681460001) until appropriate staining. Finally embryos were washed twice in MABX and fixed in MEMFA 30min at RT. To mark cortical actin in MCCs, embryos were fixed in

765 4% paraformaldehyde (PFA) in PBT (PBS + 0,1% Tween v/v) for 1h at room temperature
766 (RT), washed 3x10 min in PBT at RT, then stained with phalloidin-Alexa Fluor 555
767 (Invitrogen, 1:40 in PBT) for 4 h at RT, and washed 3x10 min in PBT at RT. Primary
768 antibodies: mouse anti-Acetylated–α-Tubulin (Clone 6-11B-1, Sigma-Aldrich, T7451,
769 1:1000), rabbit anti-γ-Tubulin (Abcam, Ab 16504, 1:500), mouse anti-γ-Tubulin (Clone
770 GTU88, Ab 11316, Abcam, 1:500), Chicken anti-GFP (AVES, GFP-1020, 1:1000), rabbit
771 anti-GFP (Torrey Pines Biolabs, TP401, 1:500), mouse anti-Centrin (Clone 20H5, EMD
772 Millipore, 04-1624, 1:500). Secondary antibodies: donkey anti-rabbit-AP (Jackson
773 ImmunoResearch, 711055152, 1:1000), Alexa Fluor 647 goat anti-mouse IgG2a (1:500;
774 Thermo Fisher Scientific, A-21241), Alexa Fluor 488 goat anti-chicken (1:500; Thermo
775 Fisher Scientific, A-11039), Alexa Fluor 568 goat anti-rabbit (1:500; Thermo Fisher
776 Scientific, A-11011).
777
778 *In situ* hybridization on *Xenopus* embryos
779 Whole-mount chromogenic *in situ* hybridization and whole-mount fluorescent *in situ*
780 hybridization (FISH) was performed as detailed by Marchal and colleagues[54], and Castillo-
781 Briceno and Kodjabachian[55], respectively. For single staining, all RNA probes were labeled
782 with digoxigenin. For FISH on section, embryos were fixed in 4% paraformaldehyde (PFA),
783 stored in methanol for at least 4 h at −20°C, then rehydrated in PBT (PBS + Tween 0.1% v/v),
784 treated with triethanolamine and acetic anhydride, incubated in increasing sucrose
785 concentrations and finally embedded with OCT (VWR Chemicals). 12µm-thick cryosections
786 were made. Double FISH on sections was an adaptation of the whole-mount FISH method.
787 80ng of *cdc20b* digoxigenin-labeled sense and antisense riboprobes and 40ng of antisense *α-*
788 *tubulin* fluorescein-labeled riboprobe[56] were used for hybridization. All probes were
789 generated from linearized plasmids using RNA-labeling mix (Roche). FISH was carried out

using Tyramide Signal Amplification – TSA TM Plus Cyanine 3/Fluorescein System (PerkinElmer). Antibodies: Anti-DigAP (Roche, 11266026, 1:5000), Anti-DigPOD (Roche, 11207733910, 1:500), Anti-FluoPOD (Roche, 11426346910, 1:500).

Microscopy

Confocal: Flat-mounted epidermal explants were examined with a Zeiss LSM 780 confocal microscope. Four-colors confocal z-series images were acquired using sequential laser excitation, converted into single plane projection and analyzed using ImageJ software. Scanning Electron Microscopy (SEM): stage 37 *Xenopus* embryos were fixed in 3% glutaraldehyde in 0.1 M phosphatase buffer pH 7.4 (19 ml monosodium phosphate 0.2 M and 81 ml disodium phosphate 0.2 M) made with filtered (0.22 µm) bi-distilled water, during 4 h with vigorous agitation, then washed with phosphatase buffer and filtered bi-distilled water, to be successively dehydrated in ethanol at 25, 50 and 70% for 30 minutes each; then, embryos were stored in fresh ethanol 70% at 4°C for 1–2 days before further processing. Embryos in 70% ethanol were further dehydrated with vigorous agitation in ethanol once at 90% and twice at 100% for 30 minutes each; they were subsequently subjected to CO2 critical point drying (CPD030, Balzers) at 31°C and 73 atm. Finally, samples were sputter-coated with gold (vacuum 1×10-12 Torr, beam energy 3–4 keV) for immediate SEM digital imaging (FEI TENEO) of the skin epidermis. Transmission Electron Microscopy (TEM): stage 25 *Xenopus* embryos were fixed overnight at 4°C in 2.5% glutaraldehyde, 2% paraformaldehyde, 0.1% tannic acid in a sodium cacodylate buffer 0.05 M pH7.3. Next, embryos were washed 3x15 min in cacodylate 0.05 M at 4°C. Post-fixation was done in 1% osmium buffer for 2 h. Next, embryos were washed in buffer for 15 min. Then, embryos were washed in water and dehydrated conventionally with alcohol, followed by a step in 70% alcohol containing 2% uranyl during 1 to 2 h at RT, or overnight at 4°C. Following 3 incubations in 100% alcohol,

completed with 3 washes of acetone, embryos were included in classical epon resin, which was polymerized in oven at 60°C for 48 h. Sections of 80 nm were made and analyzed into an FMI TECNAI microscope with acceleration of 200kV.

Statistical analysis of *Xenopus* experiments

To quantify the effect of our different experiments, we applied One-way ANOVA analysis and Bonferroni's multiple comparisons test (t test). ***P<0.05; ns = not significant. Statistical analyses were done using GraphPad Prism 6.

Fig. 5o and Fig. S6k: 10 cells per condition were analyzed and the total number of Centrin-YFP or γ-tubulin positive spots per injected cell was counted.

Fig. 7g: 5 fields (20x zoom) per condition were analyzed, and the total number of properly ciliated MCCs based on acetylated α-tubulin staining among GFP positive cells per field was counted. Each field corresponded to a different embryo.

Fig. 5s : 160-200 cells per condition were analyzed. n= 6, 8, and 10 embryos from 3 independent experiments for control, Mo ATG and Mo Spl, respectively. Unpaired t test vs control: p=0,0037 (Mo ATG **) and 0,0004 (Mo Spl ***).

Data availability statement

scRNAseq data was submitted to the GEO portal under series reference GSE103518. All other relevant data are available from the authors.

References

1. Meunier, A. & Azimzadeh, J. Multiciliated Cells in Animals. *Cold Spring Harb Perspect Biol* **8** (2016).

2. Spassky, N. & Meunier, A. The development and functions of multiciliated epithelia. *Nat Rev Mol Cell Biol* **18**, 423-436 (2017).

3. Brooks, E.R. & Wallingford, J.B. Multiciliated cells. *Curr Biol* **24**, R973-982 (2014).

4. Kyrousi, C. *et al.* Mcidas and GemC1 are key regulators for the generation of multiciliated ependymal cells in the adult neurogenic niche. *Development* **142**, 3661-3674 (2015).

5. Arbi, M. *et al.* GemC1 controls multiciliogenesis in the airway epithelium. *EMBO Rep* **17**, 400-413 (2016).

6. Terre, B. *et al.* GEMC1 is a critical regulator of multiciliated cell differentiation. *EMBO J* **35**, 942-960 (2016).

7. Zhou, F. *et al.* Gmnc Is a Master Regulator of the Multiciliated Cell Differentiation Program. *Curr Biol* **25**, 3267-3273 (2015).

8. Stubbs, J.L., Vladar, E.K., Axelrod, J.D. & Kintner, C. Multicilin promotes centriole assembly and ciliogenesis during multiciliate cell differentiation. *Nat Cell Biol* **14**, 140-147 (2012).

9. Ma, L., Quigley, I., Omran, H. & Kintner, C. Multicilin drives centriole biogenesis via E2f proteins. *Genes Dev* **28**, 1461-1471 (2014).

10. Quigley, I.K. & Kintner, C. Rfx2 Stabilizes Foxj1 Binding at Chromatin Loops to Enable Multiciliated Cell Gene Expression. *PLoS Genet* **13**, e1006538 (2017).

11. Chung, M.I. *et al.* RFX2 is broadly required for ciliogenesis during vertebrate development. *Dev Biol* **363**, 155-165 (2012).

12. Boon, M. *et al.* MCIDAS mutations result in a mucociliary clearance disorder with reduced generation of multiple motile cilia. *Nat Commun* **5**, 4418 (2014).

13. Wallmeier, J. *et al.* Mutations in CCNO result in congenital mucociliary clearance disorder with reduced generation of multiple motile cilia. *Nat Genet* **46**, 646-651 (2014).

14. Sorokin, S.P. Reconstructions of centriole formation and ciliogenesis in mammalian lungs. *J Cell Sci* **3**, 207-230 (1968).

15. Dirksen, E.R. Centriole morphogenesis in developing ciliated epithelium of the mouse oviduct. *J Cell Biol* **51**, 286-302 (1971).

16. Anderson, R.G. & Brenner, R.M. The formation of basal bodies (centrioles) in the Rhesus monkey oviduct. *J Cell Biol* **50**, 10-34 (1971).

17. Kalnins, V.I. & Porter, K.R. Centriole replication during ciliogenesis in the chick tracheal epithelium. *Z Zellforsch Mikrosk Anat* **100**, 1-30 (1969).

18. Steinman, R.M. An electron microscopic study of ciliogenesis in developing epidermis and trachea in the embryo of Xenopus laevis. *Am J Anat* **122**, 19-55 (1968).

19. Al Jord, A. *et al.* Centriole amplification by mother and daughter centrioles differs in multiciliated cells. *Nature* **516**, 104-107 (2014).

20. Klos Dehring, D.A. *et al.* Deuterosome-mediated centriole biogenesis. *Dev Cell* **27**, 103-112 (2013).

21. Zhao, H. *et al.* The Cep63 paralogue Deup1 enables massive de novo centriole biogenesis for vertebrate multiciliogenesis. *Nat Cell Biol* **15**, 1434-1444 (2013).

22. Sir, J.H. *et al.* A primary microcephaly protein complex forms a ring around parental centrioles. *Nat Genet* **43**, 1147-1153 (2011).

23. Marcet, B. *et al.* Control of vertebrate multiciliogenesis by miR-449 through direct repression of the Delta/Notch pathway. *Nat Cell Biol* **13**, 693-699 (2011).

24. Tan, F.E. *et al.* Myb promotes centriole amplification and later steps of the multiciliogenesis program. *Development* **140**, 4277-4286 (2013).

25. Yu, H. Cdc20: a WD40 activator for a cell cycle degradation machine. *Mol Cell* **27**, 3-16 (2007).

888 26. Song, R. *et al.* miR-34/449 miRNAs are required for motile ciliogenesis by repressing
889 cp110. *Nature* **510**, 115-120 (2014).
890 27. Otto, T. *et al.* Cell cycle-targeting microRNAs promote differentiation by enforcing
891 cell-cycle exit. *Proc Natl Acad Sci U S A* **114**, 10660-10665 (2017).
892 28. Wu, J. *et al.* Two miRNA clusters, miR-34b/c and miR-449, are essential for normal
893 brain development, motile ciliogenesis, and spermatogenesis. *Proc Natl Acad Sci U S A* **111**,
894 E2851-2857 (2014).
895 29. Chevalier, B. *et al.* miR-34/449 control apical actin network formation during
896 multiciliogenesis through small GTPase pathways. *Nat Commun* **6**, 8386 (2015).
897 30. Mercey, O. *et al.* Characterizing isomiR variants within the microRNA-34/449 family.
898 *FEBS Lett* **591**, 693-705 (2017).
899 31. Firat-Karalar, E.N., Rauniyar, N., Yates, J.R., 3rd & Stearns, T. Proximity interactions
900 among centrosome components identify regulators of centriole duplication. *Curr Biol* **24**,
901 664-670 (2014).
902 32. Robu, M.E. *et al.* p53 activation by knockdown technologies. *PLoS Genet* **3**, e78
903 (2007).
904 33. Werner, M.E. *et al.* Radial intercalation is regulated by the Par complex and the
905 microtubule-stabilizing protein CLAMP/Spef1. *J Cell Biol* **206**, 367-376 (2014).
906 34. Firat-Karalar, E.N. & Stearns, T. The centriole duplication cycle. *Philos Trans R Soc*
907 *Lond B Biol Sci* **369** (2014).
908 35. Tsou, M.F. *et al.* Polo kinase and separase regulate the mitotic licensing of centriole
909 duplication in human cells. *Dev Cell* **17**, 344-354 (2009).
910 36. Kim, J., Lee, K. & Rhee, K. PLK1 regulation of PCNT cleavage ensures fidelity of
911 centriole separation during mitotic exit. *Nat Commun* **6**, 10076 (2015).

912 37. Matsuo, K. *et al.* Kendrin is a novel substrate for separase involved in the licensing of
913 centriole duplication. *Curr Biol* **22**, 915-921 (2012).
914 38. Al Jord, A. *et al.* Calibrated mitotic oscillator drives motile ciliogenesis. *Science* **358**,
915 803-806 (2017).
916 39. Huttlin, E.L. *et al.* The BioPlex Network: A Systematic Exploration of the Human
917 Interactome. *Cell* **162**, 425-440 (2015).
918 40. Rual, J.F. *et al.* Towards a proteome-scale map of the human protein-protein
919 interaction network. *Nature* **437**, 1173-1178 (2005).
920 41. Thein, K.H., Kleylein-Sohn, J., Nigg, E.A. & Gruneberg, U. Astrin is required for the
921 maintenance of sister chromatid cohesion and centrosome integrity. *J Cell Biol* **178**, 345-354
922 (2007).
923 42. Chiu, S.C. *et al.* The mitosis-regulating and protein-protein interaction activities of
924 astrin are controlled by aurora-A-induced phosphorylation. *Am J Physiol Cell Physiol* **307**,
925 C466-478 (2014).
926 43. Eguren, M. *et al.* The APC/C cofactor Cdh1 prevents replicative stress and p53-
927 dependent cell death in neural progenitors. *Nat Commun* **4**, 2880 (2013).
928 44. Chung, H.J., Park, J.E., Lee, N.S., Kim, H. & Jang, C.Y. Phosphorylation of Astrin
929 Regulates Its Kinetochore Function. *J Biol Chem* **291**, 17579-17592 (2016).
930 45. Qiu, X. *et al.* Single-cell mRNA quantification and differential analysis with Census.
931 *Nat Methods* **14**, 309-315 (2017).
932 46. Macosko, E.Z. *et al.* Highly Parallel Genome-wide Expression Profiling of Individual
933 Cells Using Nanoliter Droplets. *Cell* **161**, 1202-1214 (2015).
934 47. Kim, D. *et al.* TopHat2: accurate alignment of transcriptomes in the presence of
935 insertions, deletions and gene fusions. *Genome Biol* **14**, R36 (2013).

48. Anders, S., Pyl, P.T. & Huber, W. HTSeq--a Python framework to work with high-throughput sequencing data. *Bioinformatics* **31**, 166-169 (2015).

49. Love, M.I., Huber, W. & Anders, S. Moderated estimation of fold change and dispersion for RNA-seq data with DESeq2. *Genome Biol* **15**, 550 (2014).

50. Langmead, B. & Salzberg, S.L. Fast gapped-read alignment with Bowtie 2. *Nat Methods* **9**, 357-359 (2012).

51. Heinz, S. *et al.* Simple combinations of lineage-determining transcription factors prime cis-regulatory elements required for macrophage and B cell identities. *Mol Cell* **38**, 576-589 (2010).

52. Boutin, C. *et al.* NeuroD1 induces terminal neuronal differentiation in olfactory neurogenesis. *Proc Natl Acad Sci U S A* **107**, 1201-1206 (2010).

53. Boutin, C., Diestel, S., Desoeuvre, A., Tiveron, M.C. & Cremer, H. Efficient in vivo electroporation of the postnatal rodent forebrain. *PLoS One* **3**, e1883 (2008).

54. Marchal, L., Luxardi, G., Thome, V. & Kodjabachian, L. BMP inhibition initiates neural induction via FGF signaling and Zic genes. *Proc Natl Acad Sci U S A* **106**, 17437-17442 (2009).

55. Castillo-Briceno, P. & Kodjabachian, L. Xenopus embryonic epidermis as a mucociliary cellular ecosystem to assess the effect of sex hormones in a non-reproductive context. *Front Zool* **11**, 9 (2014).

56. Deblandre, G.A., Wettstein, D.A., Koyano-Nakagawa, N. & Kintner, C. A two-step mechanism generates the spacing pattern of the ciliated cells in the skin of Xenopus embryos. *Development* **126**, 4715-4728 (1999).

Acknowledgements

960 We are grateful to Chris Kintner, Marc Kirschner, Olaf Stemmann, Reinhard Köster, Xavier
961 Morin and Xueliang Zhu for reagents. Imaging in IBDM was performed on PiCSL-FBI core
962 facility, supported by the French National Research Agency through the program
963 "Investments for the Future" (France-BioImaging, ANR-10-INBS-04). Sequencing at
964 UCAGenomiX (IPMC), a partner of the National Infrastructure France Génomique, was
965 supported by Commissariat aux Grands Investissements (ANR-10-INBS-09-03, ANR-10-
966 INBS-09-02) and Canceropôle PACA. The authors thank Florian Roguet for *Xenopus* care,
967 and Nathalie Garin from Leica Microsystems GmbH for technical advice on STED
968 microscopy. We are grateful to Rainer Waldmann, Kévin Lebrigand, Virginie Magnone and
969 Nicolas Nottet for fruitful discussions on single cell RNA sequencing, and Delphine Debayle
970 for help with mass spectrometry experiments. We thank Julien Royet and Harold Cremer for
971 insightful comments on the manuscript. This project was funded by grants from ANR (ANR-
972 11-BSV2-021-02, ANR-13-BSV4-0013, ANR-15-CE13-0003), FRM (DEQ20141231765,
973 DEQ20130326464, DEQ20180339158), Fondation ARC (PJA 20161204865, PJA
974 20161204542), the labex Signalife (ANR-11-LABX-0028-01), the association Vaincre la
975 Mucoviscidose (RF20140501158, RF20120600738, RF20150501288), and the Chan
976 Zuckerberg Initiative (Silicon Valley Fundation, 2017-175159 -5022). OM, CB and DRR were
977 supported by fellowships from Ligue Nationale contre le Cancer (OM and CB), and Fondation
978 ARC (DRR).
979

980 **Author contributions**

981 PB, BM and LK designed and supervised the study, and obtained funding. LEZ, SRG, OM
982 performed and analyzed human and mouse airway cells experiments. DRR and VT performed
983 and analyzed *Xenopus* experiments. CB performed and analyzed all experiments on mouse
984 ependymal MCCs and contributed to the description of *Xenopus* deuterosomes. OR

characterized CDC20B antibodies. MD and AP performed the bioinformatic analysis. NP carried out scRNAseq experiments. ASG performed mass spectrometry analyses. GP designed and performed CDC20B interaction studies. All authors were involved in data interpretation. DRR, LEZ and CB designed the figures. LK drafted the original manuscript. DRR, LEZ, CB, BM, PB and LK edited the manuscript.

Competing financial interests

The authors declare no competing interests.

Figures and legends

Figure 1: Single-cell RNA-seq analysis reveals MCC transcriptome at deuterosome-stage.

(**a**) Experimental design of the scRNA-seq experiment. (**b**) tSNE plot. Each point is a projection of a unique cell on a 2D space generated by the tSNE algorithm. Blue dots represent *MKI67*-positive proliferating cells, and red dots represent *DEUP1*-positive cells corresponding to maturing MCCs at deuterosome stage. (**c**) Cell cycle-related gene set expression in HAECs measured by scRNA-seq. Cells were ordered along a pseudotime axis, defined with the Monocle2 package. Phase specific scores are displayed in the top heatmap. Expression of selected genes is displayed in the bottom heatmap. (**d**) tSNEs plots for a selection of genes specifically enriched in deuterosome-stage cells. Note that *CDC20B* exhibits the most specific expression among deuterosome marker genes.

Figure 2: Composition and organization of vertebrate deuterosomes

(**a-b**) Maturing mouse ependymal MCCs were immunostained as indicated, pictures were taken with confocal (**a**) or STED (**b**) microscope. (**a**) DEUP1 stains the deuterosome core (ring) and a close fibrous area that defines the perideuterosomal region. The centriolar marker FOP reveals procentrioles arranged in a circle around the deuterosome. Pericentrin (PCNT) is enriched in the perideuterosomal region. γ-Tubulin (γ-TUB) stains the core as well as the periphery of the deuterosome. (**b**) STED pictures showing the organization of FOP, PCNT and γ-TUB around deuterosomes. Individual centrioles identified by FOP staining are pointed out with arrowheads. The diagram was drawn from the adjacent FOP photograph to help reveal the regular concentric organization of nascent centrioles in a typical deuterosomal figure. (**c**) *Xenopus* embryos were immunostained for γ-Tubulin (γ-Tub) and Centrin and high-magnification pictures of immature epidermal MCCs were taken. In these cells, Centrin-positive procentrioles grow around γ-Tubulin positive structures. (**d**) *Xenopus* embryos were

injected with *Multicilin-hGR* and *GFP-Deup1* mRNAs, treated with dexamethasone at gastrula st11 to induce Multicilin activity, and immunostained at neurula st18 for γ-Tubulin, GFP and Centrin. Scale bars: 5µm (**a**, top), 500nm (**a**, bottom), 500nm (**b**), 10µm (**c**, **d**, large view), 1µm (**c**, **d**, high magnification).

Figure 3: CDC20B associates to vertebrate deuterosomes.

(**a**) Double immunofluorescence was performed on mouse tracheal MCCs after 3 days of culture in air-liquid interface. Low magnification confocal panels show coincident CDC20B and DEUP1 staining in several individual MCCs. High magnification on a single MCC reveals the prominent association of CDC20B to large deuterosomes marked by DEUP1 (arrowheads). Note that some smaller deuterosomes do not contain CDC20B (arrows). (**b**) Mouse ependymal MCCs were immunostained as indicated, and high magnification confocal pictures of cells with immature and mature deuterosomal figures were taken. In these cells, centrioles revealed by FOP form a ring around deuterosomes. CDC20B staining forms a ring inside the ring of FOP-positive procentrioles indicating that CDC20B is tightly associated to deuterosomes. Note that the CDC20B signal associated to deuterosome increased with their maturation (high-magnification pictures of >25 cells per category from two different animals were quantified in the graph; horizontal bars are mean values and vertical lines are standard deviations). Unpaired t test vs immature: p=0,0005 (intermediate, ***); p<0,0001 (mature, ****). (**c**) *Xenopus* embryos were injected with *GFP-Deup1* mRNA and immunostained at neurula st18 as indicated. Scale bars: 5µm (**a**, **b**, large view), 1.5µm (**a**, high magnification), 500nm (**b**, high magnification), 10µm (**c**).

Figure 4: CDC20B knockdown impairs multiciliogenesis in mouse ependymal MCCs.

(**a**,**b**) Ependyma were stained for CDC20B (green) and FOXJ1 (nuclear MCC fate marker, red) 5 days post electroporation (5dpe) of control shRNA (**a**) or *Cdc20b* shRNA (**b**). sh277 is exemplified here, but all three *Cdc20b* shRNAs produced similar effects. (**c**) Graph showing the quantification of CDC20B protein levels in cells at the deuterosomal stage at 5dpe from two experiments. Horizontal lines are mean values and vertical lines are standard error mean. Unpaired t test: $p<0.0001$ (sh273, sh274, sh277, ****). (**d**) Histogram showing the number of FOXJ1-positive nuclei observed for each field (dot), with mean values (horizontal lines) and standard deviations (vertical lines) from two experiments. Unpaired t test: 0.3961 (sh273, ns), 0.1265 (sh274, ns), 0.3250 (sh277, ns). No significant variations were observed between conditions, indicating that MCC fate acquisition was not affected by *Cdc20b* knockdown. (**e-f**) Confocal pictures of 9dpe ependyma electroporated with control shRNA (**e**) or *Cdc20b* shRNAs (**f**) and stained for DEUP1 (deuterosome, green), FOP (centrioles, red) and ZO1 (cell junction, white). DEUP1 positive deuterosomes with non-disengaged FOP positive centrioles were observed much more frequently in MCCs electroporated with *Cdc20b* shRNAs compared to control. (**g**) Histogram showing the percentage of MCCs with non-disengaged centrioles per field (dots), with mean values (horizontal bars) and standard deviations (vertical lines). Two experiments were analyzed. Unpaired t test: $p<0.0001$ (sh273, sh274, sh277, ****). (**h-i**) Confocal pictures of 15dpe ependyma stained for FOP (centrioles, green), α-Tubulin (α-TUB, cilia, red) and ZO1 (cell junction, white) showing the morphology of normal MCCs in shRNA control condition (**h**), and examples of defects observed in MCCs treated with sh *Cdc20b* (**i**). (**j**) Histogram showing the number of released centrioles per cell (dots), with mean values (horizontal bars) and standard deviations (vertical lines). (**k**) Bar graph showing the percentage of normal and abnormal MCCs. MCCs were scored abnormal when they did not display organized centriole patches associated to cilia. Three experiments

were analyzed. Unpaired t test: p=0.0004 (sh273, ***), 0.0001 (sh274, ****), 0.0038 (sh277, **). Scale bars: 20µm (**a**), 5µm (**e**, **i**).

Figure 5: *cdc20b* knockdown impairs multiciliogenesis in *Xenopus* epidermal MCCs.

(**a-c**) 8-cell embryos were injected in presumptive epidermis with *GFP-CAAX* mRNA and *cdc20b* morpholinos, as indicated. Embryos at tailbud st25 were processed for fluorescent staining against GFP (injection tracer, green) and Acetylated-α-Tubulin (Ac-α-Tub, cilia, white). White dotted lines indicate the position of orthogonal projections shown in bottom panels. Note that *cdc20b* morphant MCCs display cytoplasmic filaments but do not grow cilia (white arrowheads). (**d-f**) Scanning Electron Microscopy (SEM) of control (**d**) and *cdc20b* morphant (**e**,**f**) embryos at tadpole st31. Yellow arrowheads point at normal (**d**) and defective MCCs (**e**,**f**). (**g-i**) Transmission Electron Microscopy (TEM) of control (**g**) and *cdc20b* morphant (**h**,**i**) embryos at tailbud st25. Yellow arrowheads point at normally docked basal bodies supporting cilia (**g**) and undocked centrioles unable to support cilia (**h**,**i**). (**j-n**) 8-cell embryos were injected in presumptive epidermis with *centrin-YFP* mRNA, *cdc20b* morpholinos, and *cdc20b* mRNA, as indicated. Centrin-YFP fluorescence was observed directly to reveal centrioles (yellow). Nuclei were revealed by DAPI staining in blue. White dotted lines indicate the position of orthogonal projections shown in bottom panels. Yellow arrowheads point at undocked centrioles. (**o**) Bar graph showing the number of BBs per MCC, and standard error mean, as counted by Centrin-YFP dots. One way ANOVA and Bonferroni's Multiple Comparisons Test on two experiments, *** = p<0.0001. *cdc20b* knockdown significantly reduced the number of BBs per cell, and this defect could be corrected by *cdc20b* co-injection with Mo Spl. (**p-u**) Embryos were injected with *Multicilin-hGR* and *GFP-Deup1* mRNAs, treated with dexamethasone at gastrula st11 to induce Multicilin activity, and immunostained at neurula st23 against Acetylated-α-tubulin (cilia,

white), GFP (deuterosomes, green) and Centrin (centrioles, red). (**p**) Control cells showed individual centrioles, many of which had initiated ciliogenesis. Note that Deup1-positive deuterosomes were no longer visible at this stage. (**q**,**r**,**t**,**u**) *cdc20b* morphant MCCs showed procentrioles still engaged on deuterosomes and lacked cilia. (**s**) bar graph showing the percentage of cells that completed or not centriole disengagement with standard deviations (vertical lines). Three experiments were analyzed. Unpaired t test: p=0,0037 (Mo ATG, **), 0,0004 (Mo Spl, ***). Scale bars: 20µm (**a**, **d**), 1µm (**g**, **t**), 5µm (**j**, **p**).

Figure 6: CDC20B interacts with PLK1, SPAG5 and DEUP1

(**a**, **c**, **e**) Co-immunoprecipitations of PLK1, SPAG5 and DEUP1 with CDC20B were tested after transfections of different constructs in HEK cells, indicated at the top of each panel. Proteins (left legend) were revealed by immunoblotting. (**b**, **d**) Maturing mouse ependyma were immunostained for the indicated proteins, and pictures were taken with a confocal microscope. PLK1 and SPAG5 are expressed in maturing MCCs. High magnifications show that PLK1 is enriched in the perideuterosomal region, while SPAG5 is enriched in the deuterosome core. Scale bars: 5µm (**d**, **e**, large view), 1µm (**d**, **e**, high magnification).

Figure 7: Separase overexpression rescues multiciliogenesis in absence of Cdc20b.

(**a-f**) 8-cell *Xenopus* embryos were injected in the presumptive epidermis with *GFP-gpi* mRNA, *cdc20b* morpholinos, and human *Separase* mRNA, as indicated. Embryos were fixed at tailbud st25 and immunostained against GFP (injection tracer, green), Acetylated-α-Tubulin (cilia, white) and ɣ-Tubulin (BBs, red). White dotted lines indicate the position of orthogonal projections shown in bottom panels. Red arrowheads point undocked BBs. Left inset in (**e**) shows zoom on clustered centrioles. (**g**) Bar graph showing the number of properly ciliated MCCs among injected cells, per field of observation. Bars are standard error

mean. Counting was performed on pictures taken at low magnification (20x), in order to score a large number of cells. Separase overexpression fully rescued multiciliogenesis in *cdc20b* morphant MCCs. One way ANOVA and Bonferroni's Multiple Comparisons on two experiments, *** = $p<0.0001$; ns = $p>0.05$. Scale bars: 5µm **(a)**. (**h**) Model illustrating the analogy between centriole disengagement in mitotic cells and centriole release from deuterosomes in post-mitotic MCCs.

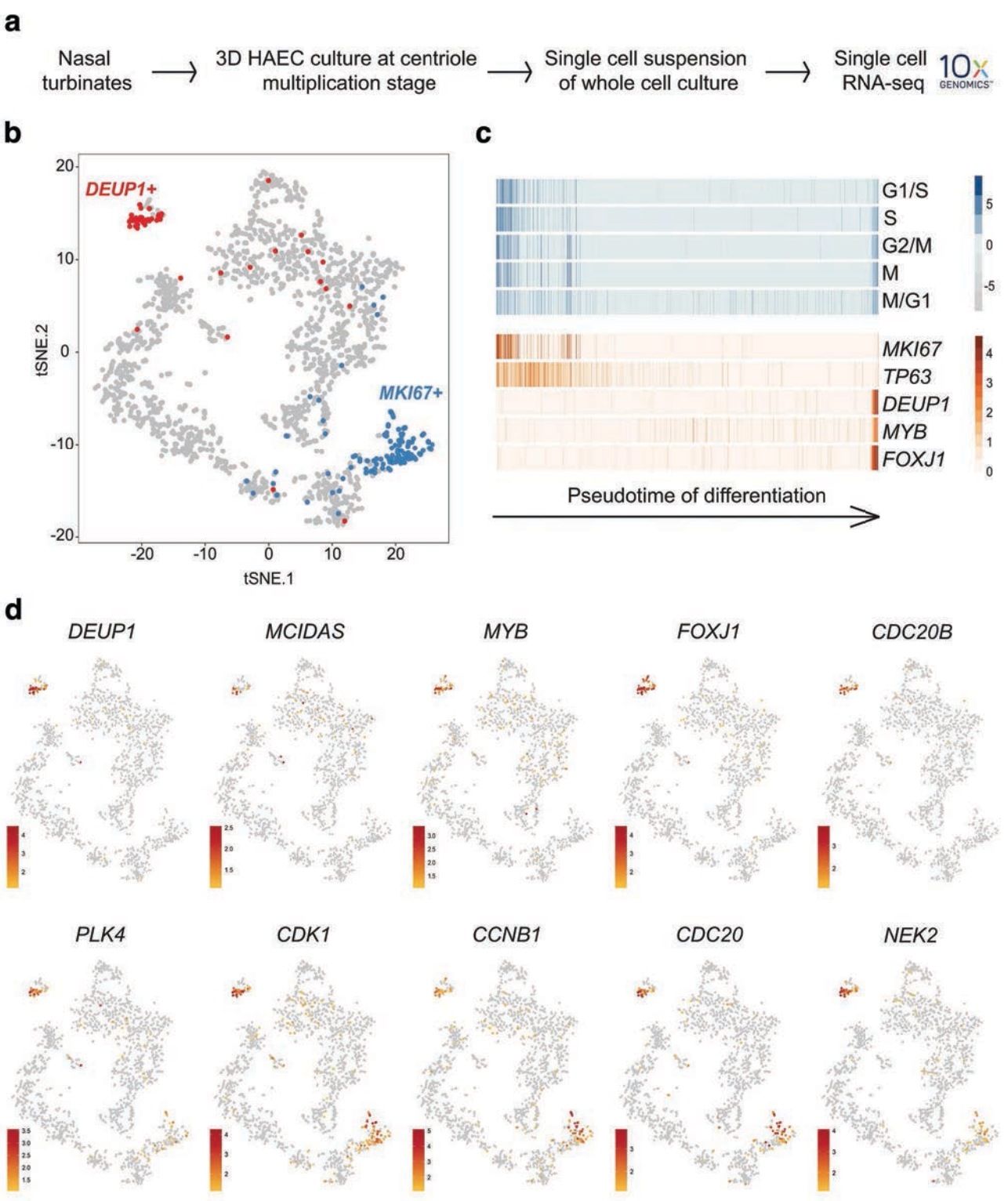
a
Nasal turbinates
3D HAEC culture at centriole multiplication stage
Single cell suspension of whole cell culture
Single cell RNA-seq
10X GENOMICS
b
DEUP1+
MKI67+
tSNE.2
tSNE.1
c
G1/S
S
G2/M
M
M/G1
MKI67
TP63
DEUP1
MYB
FOXJ1
Pseudotime of differentiation
d
DEUP1
MCIDAS
MYB
FOXJ1
CDC20B
PLK4
CDK1
CCNB1
CDC20
NEK2

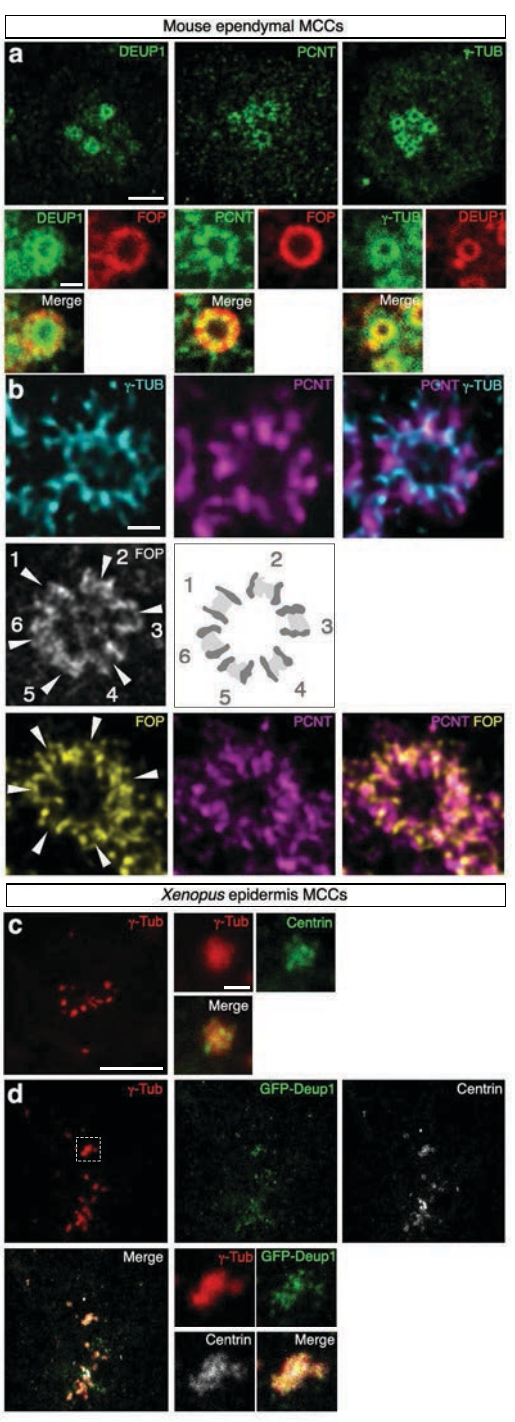
Mouse ependymal MCCs
a
DEUP1
PCNT
γ-TUB
DEUP1
FOP
PCNT
FOP
γ-TUB
DEUP1
Merge
Merge
Merge
b
γ-TUB
PCNT
PCNT γ-TUB
1
2
FOP
6
3
5
4
2
1
3
6
5
4
FOP
PCNT
PCNT FOP
Xenopus epidermis MCCs
c
γ-Tub
γ-Tub
Centrin
Merge
d
γ-Tub
GFP-Deup1
Centrin
Merge
γ-Tub
GFP-Deup1
Centrin
Merge

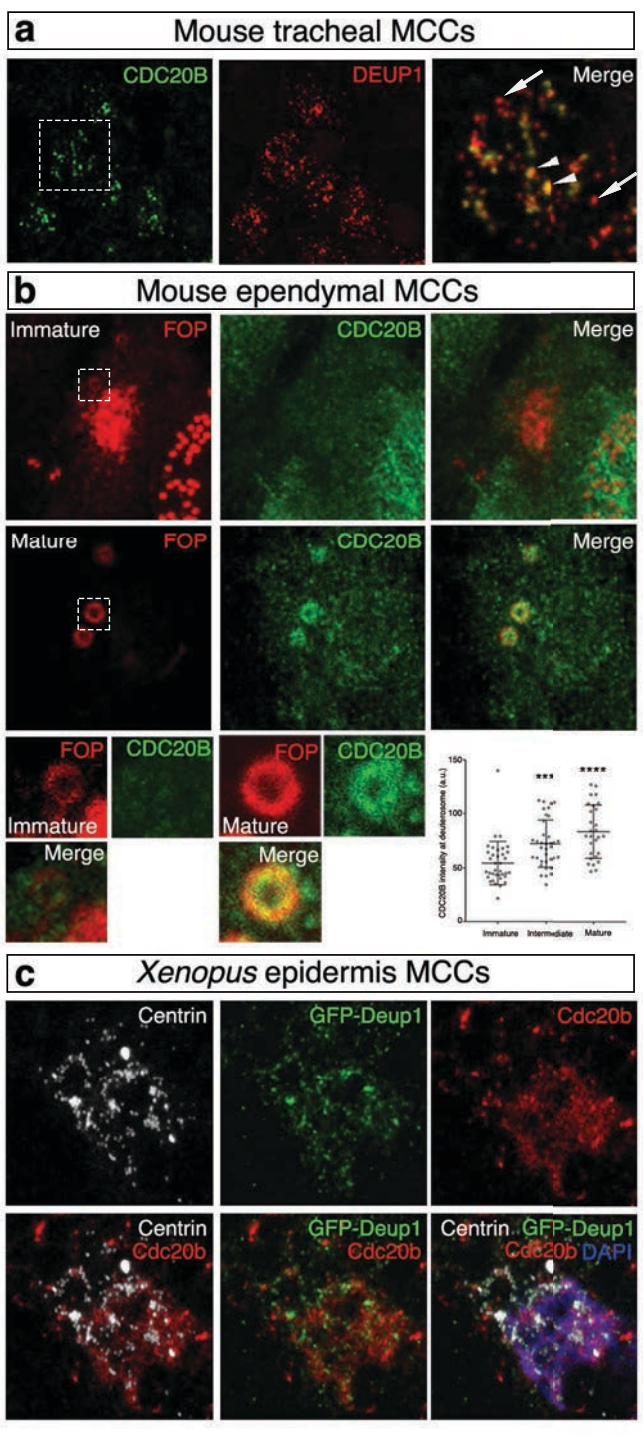
a
Mouse tracheal MCCs
CDC20B
DEUP1
Merge
b
Mouse ependymal MCCs
Immature
FOP
CDC20B
Merge
Mature
FOP
CDC20B
Merge
FOP
CDC20B
Immature
Merge
FOP
CDC20B
Mature
Merge
CDC20B intensity at deuterosome (a.u.)
150
100
50
0
***
****
Immature
Intermediate
Mature
c
Xenopus epidermis MCCs
Centrin
GFP-Deup1
Cdc20b
Centrin
Cdc20b
GFP-Deup1
Cdc20b
Centrin
GFP-Deup1
Cdc20b
DAPI

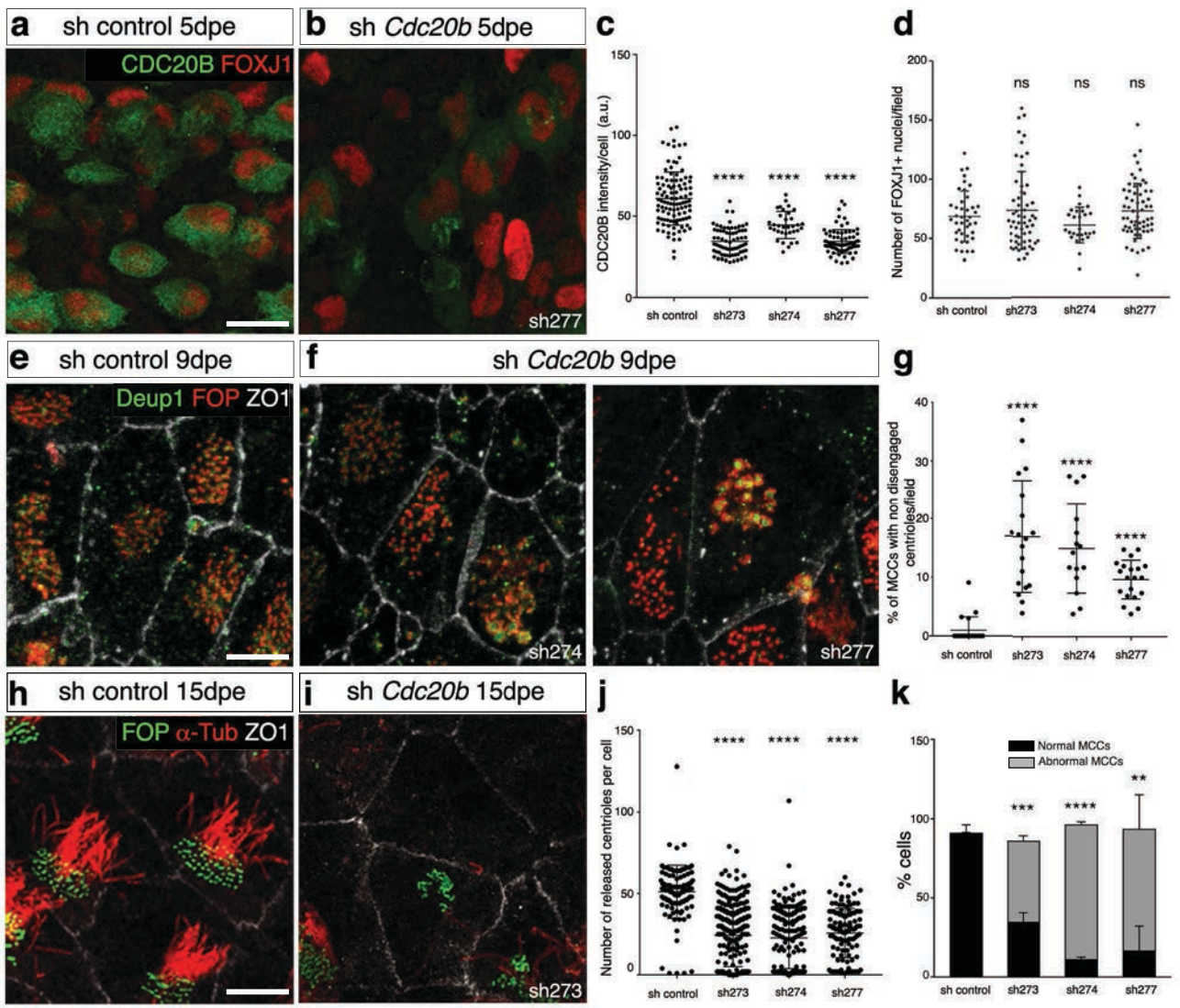
a
sh control 5dpe
CDC20B FOXJ1
b
sh Cdc20b 5dpe
sh277
c
CDC20B intensity/cell (a.u.)
150
100
50
0
****
****
****
sh control
sh273
sh274
sh277
d
Number of FOXJ1+ nuclei/field
200
150
100
50
0
ns
ns
ns
sh control
sh273
sh274
sh277
e
sh control 9dpe
Deup1 FOP ZO1
f
sh Cdc20b 9dpe
sh274
sh277
g
% of MCCs with non disengaged centrioles/field
40
30
20
10
0
****
****
****
sh control
sh273
sh274
sh277
h
sh control 15dpe
FOP α-Tub ZO1
i
sh Cdc20b 15dpe
sh273
j
Number of released centrioles per cell
150
100
50
0
****
****
****
sh control
sh273
sh274
sh277
k
Normal MCCs
Abnormal MCCs
% cells
150
100
50
0
***
****
**
sh control
sh273
sh274
sh277

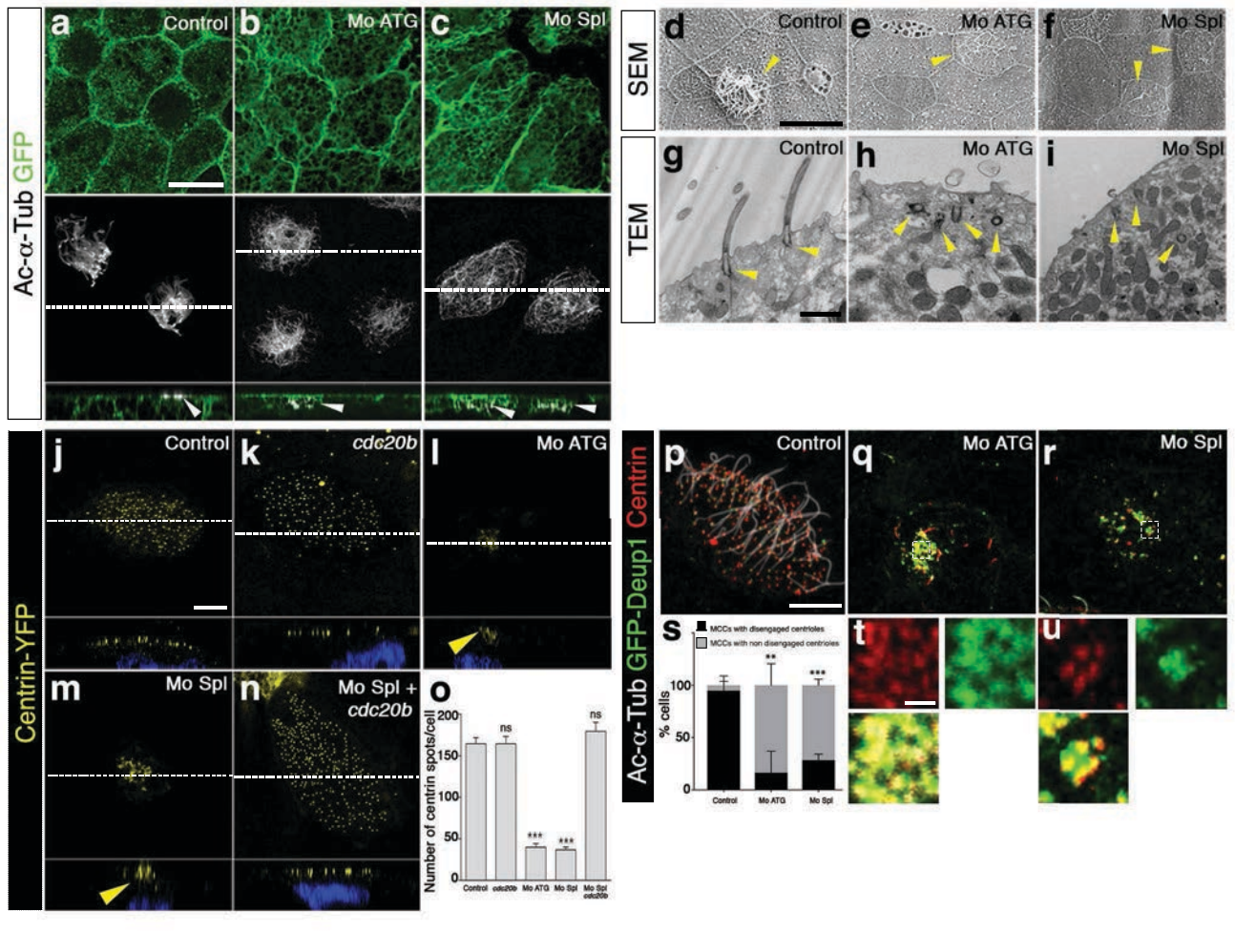
a
Control
b
Mo ATG
c
Mo Spl
Ac-α-Tub GFP
d
Control
e
Mo ATG
f
Mo Spl
SEM
g
Control
h
Mo ATG
i
Mo Spl
TEM
j
Control
k
cdc20b
l
Mo ATG
m
Mo Spl
n
Mo Spl +
cdc20b
Centrin-YFP
o
Number of centrin spots/cell
200
150
100
50
0
ns
ns
***
***
Control
cdc20b
Mo ATG
Mo Spl
Mo Spl
cdc20b
p
Control
q
Mo ATG
r
Mo Spl
Ac-α-Tub GFP-Deup1 Centrin
s
MCCs with disengaged centrioles
MCCs with non disengaged centrioles
% cells
100
50
0
**
***
Control
Mo ATG
Mo Spl
t
u

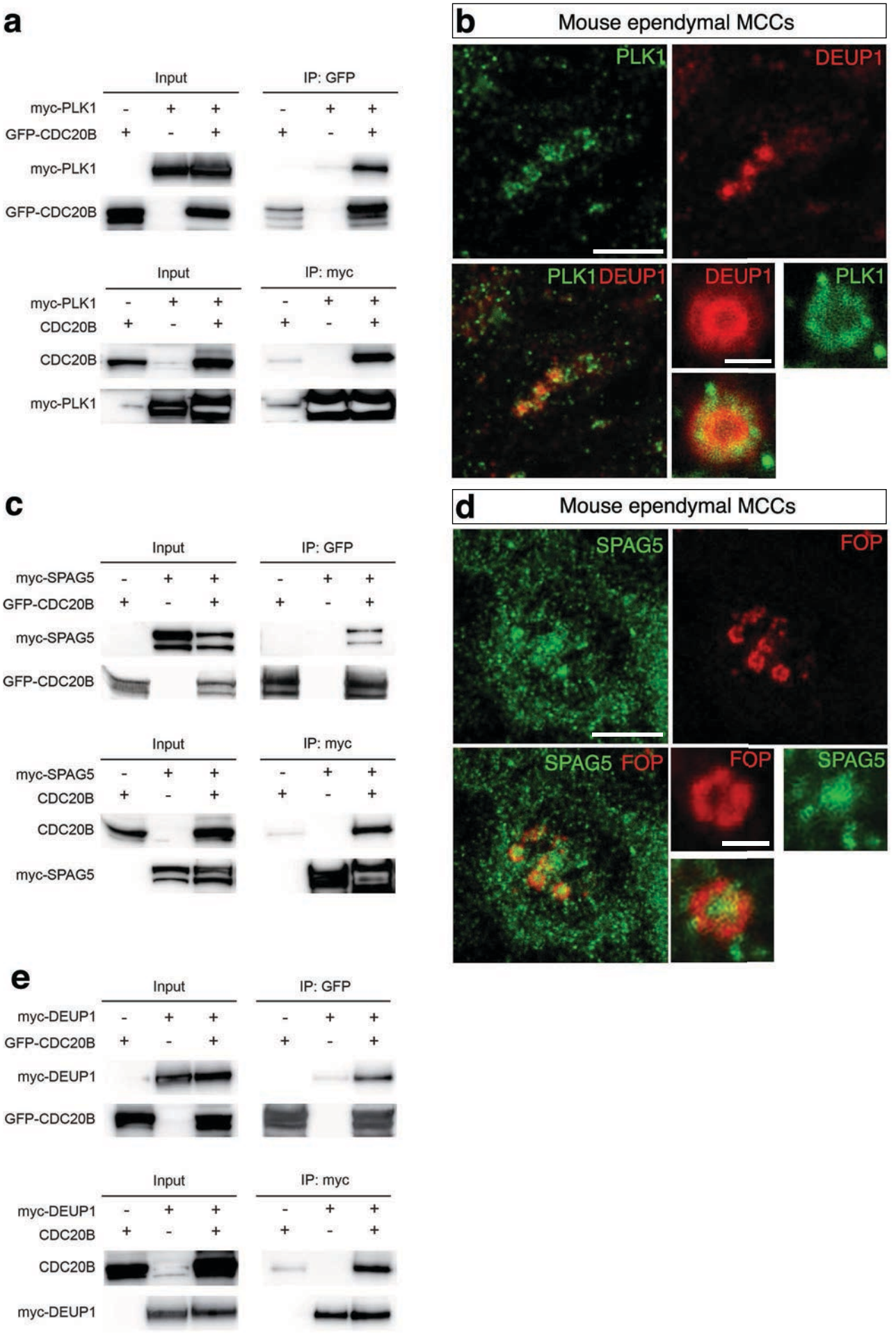
a
Input
IP: GFP
myc-PLK1
GFP-CDC20B
Input
IP: myc
CDC20B
b
Mouse ependymal MCCs
PLK1
DEUP1
PLK1 DEUP1
c
myc-SPAG5
d
SPAG5
FOP
SPAG5 FOP
e
myc-DEUP1

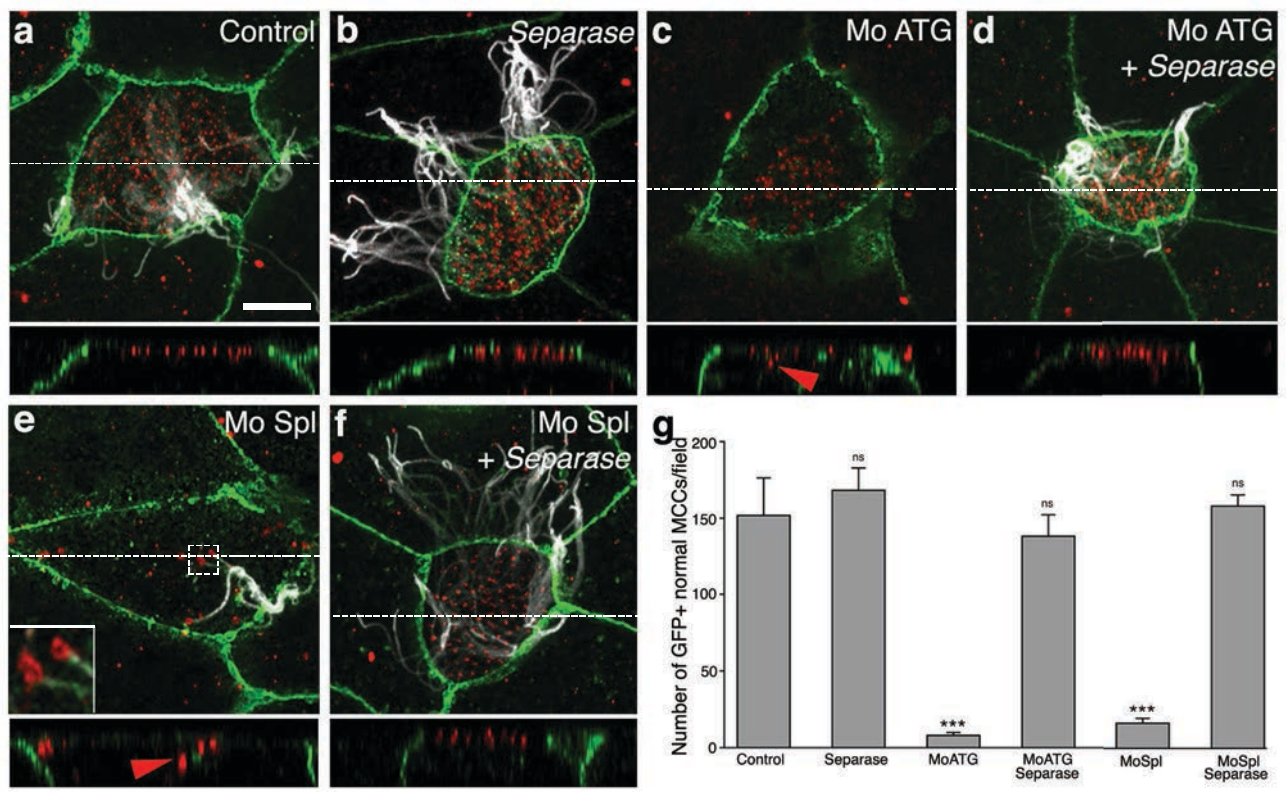

h *Centriole disengagement in mitotic cells* *Centriole release from deuterosome in post-mitotic MCCs*

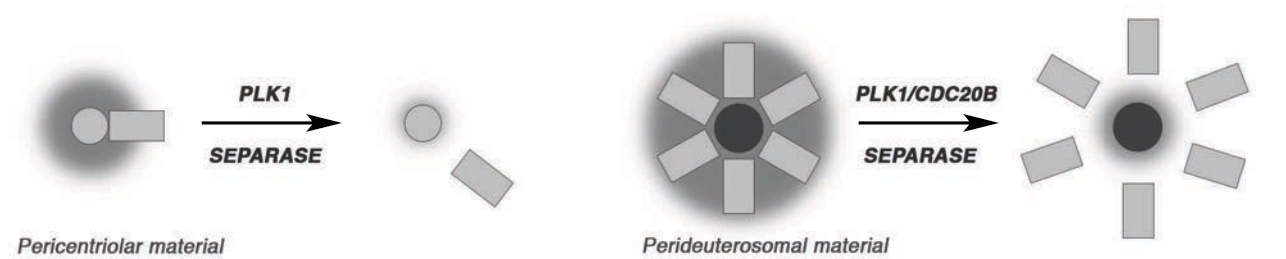

Supplementary information

CDC20B is required for deuterosome-mediated centriole production in multiciliated cells

Revinski et al.

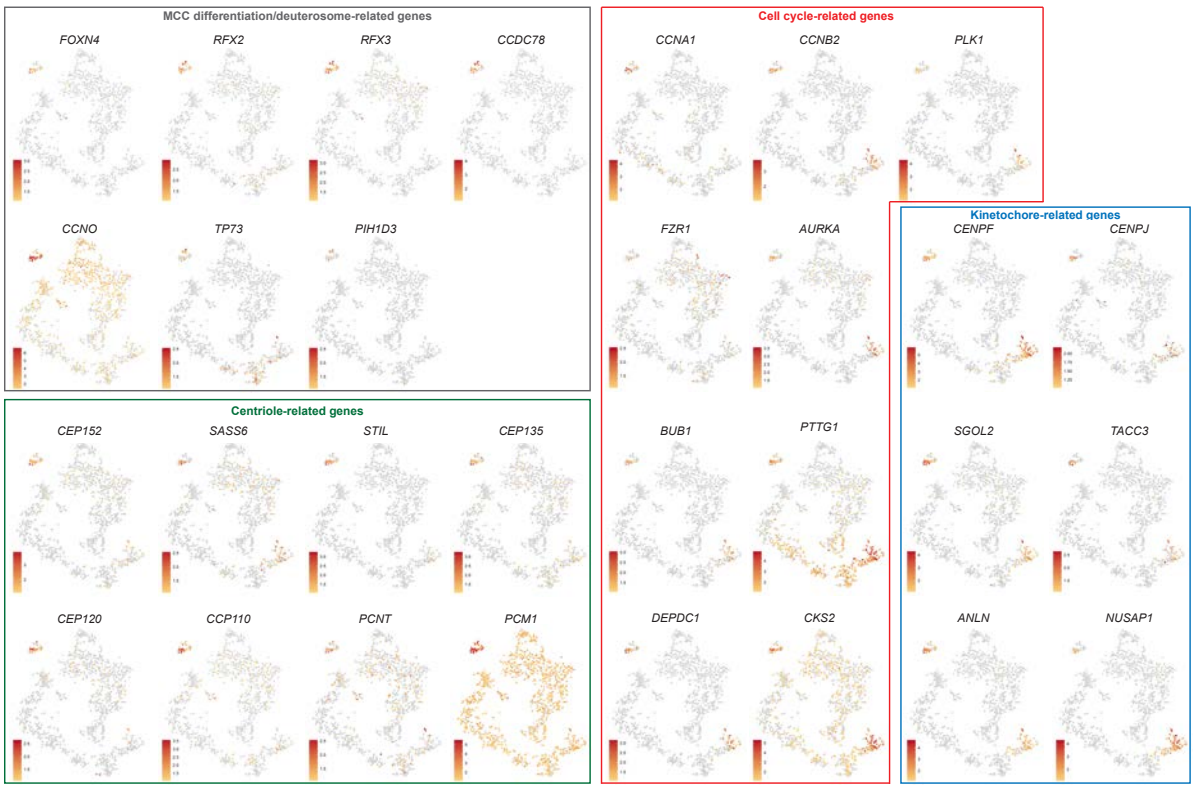

Supplementary Figure 1: Single cell RNA-seq analysis of HAECs.

tSNE plots for a selection of genes expressed at the single-cell level, in deuterosomal-stage differentiating HAECs. Genes were grouped into functional categories.

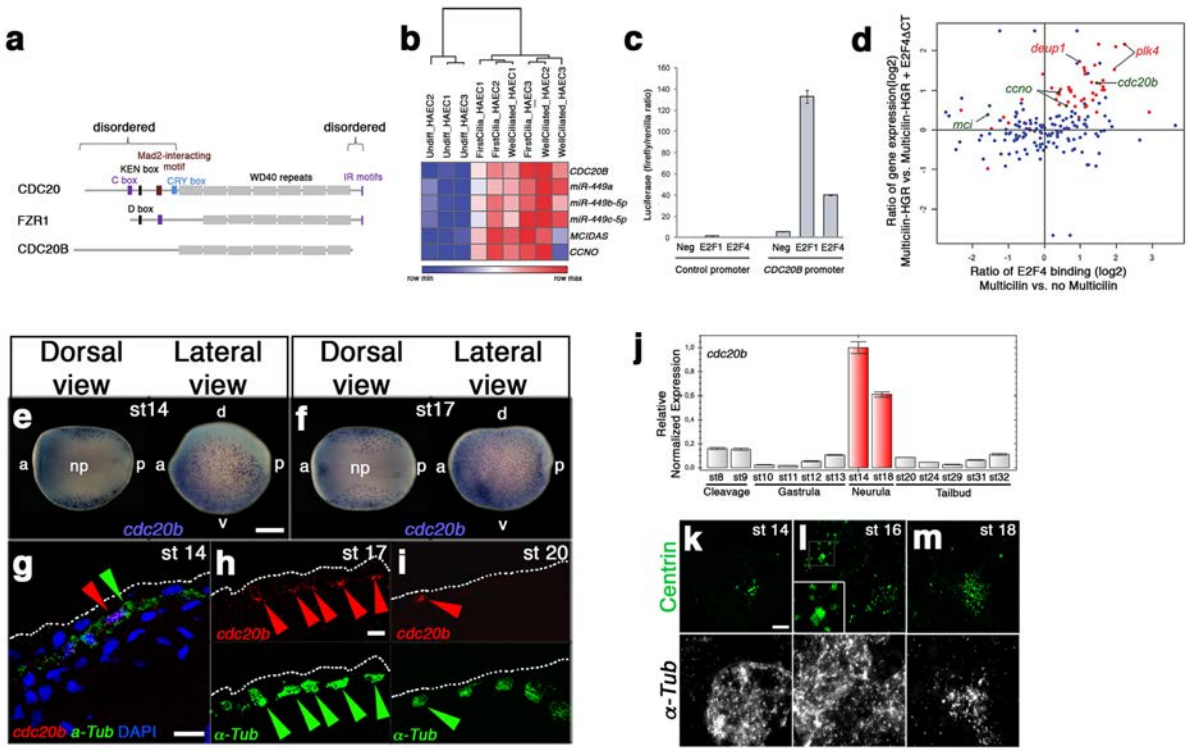

Supplementary Figure 2: Structure, regulation and spatio-temporal expression of *cdc20b*.

(a) Domain composition of CDC20 family members. The C box and IR motifs in CDC20 and FZR1 serve as APC/C binding domains. The KEN box and the Cry box in CDC20, and the D box in FZR1 are involved in their regulation by degradation. The Mad2-interacting motif in CDC20 is important for its regulation by the spindle assembly checkpoint. WD40 repeats are involved in substrate recognition. Note that CDC20B lacks degradation motifs and the APC/C binding domains present in CDC20 and FZR1. **(b)** Heatmap of gene expression measured by RNA-seq or small RNA-seq on 3 independent HAEC differentiation time courses (HAEC1 to HAEC3). Normalized read counts were Log2-transformed and median-centered by gene. Hierarchical clustering (Euclidian distance) was performed on samples. The scale color bar indicates the minimum and maximum values per row. (**c**) Promoter luciferase reporter assay. Promoter-associated firefly luciferase was normalized to constitutive renilla luciferase. Control and *CDC20B* promoter were co-expressed with a plasmid expressing E2F1 or E2F4, or a negative control. Bars represent the average of 3 independent experiments. Error bars represent

the standard deviation. (**d**) Ratio of gene expression (Multicilin-HGR vs. Multicilin-HGR +E2F4ΔCT) vs. ratio of E2F4 binding (Multicilin vs. no Multicilin). E2F4ΔCT prevents the formation of transcriptionally active Multicilin/E2F complexes. Centriole-related genes are highlighted in red. Genes from the multiciliary locus are highlighted in green. The graph was built by mapping and quantifying previously published raw data[9]. (**e**,**f**) *cdc20b* whole-mount *in situ* hybridization in early *Xenopus laevis* neurula st14 and st17, respectively. *cdc20b* mRNA is expressed in epidermal cells but not in the neural plate (np), as revealed on dorsal views. a: anterior, p: posterior, d: dorsal, v: ventral. (**g**-**i**) *cdc20b* (red) and *α-Tubulin* (α-*Tub,* green) double fluorescent *in situ* hybridization (FISH) on sectioned embryos at st14 (**g**), st17 (**h**) and st20 (**i**). Red and green arrows point immature MCCs co-expressing *cdc20b* and *α-Tub*. Nuclei are revealed by DAPI staining in blue. White dotted lines indicate the surface of the epidermis. Note that the majority of MCCs become negative for *cdc20b* expression at st20. (**j**) RT-qPCR showing the relative expression of *cdc20b* from st8 (mid-blastula transition) until tadpole st32 normalized to *ODC* expression. Red bars indicate the peak of *cdc20b* transcript accumulation between st14 and st18, when centriole amplification occurs. (**k**-**m**) To reveal the dynamics of centriole multiplication, MCCs were stained by α-*Tub* FISH and by immunostaining against Centrin. Multiple Centrin-positive foci were detected at st14, marking the onset of centriologenesis. Procentriole aggregates, presumably organized around deuterosomes were clearly visualized at st16 (inset). Dispersed multiple centrioles were detected at st18. Scale bars: 250µm (**e**), 20µm (**g**,**h**), 5µm (**k**).

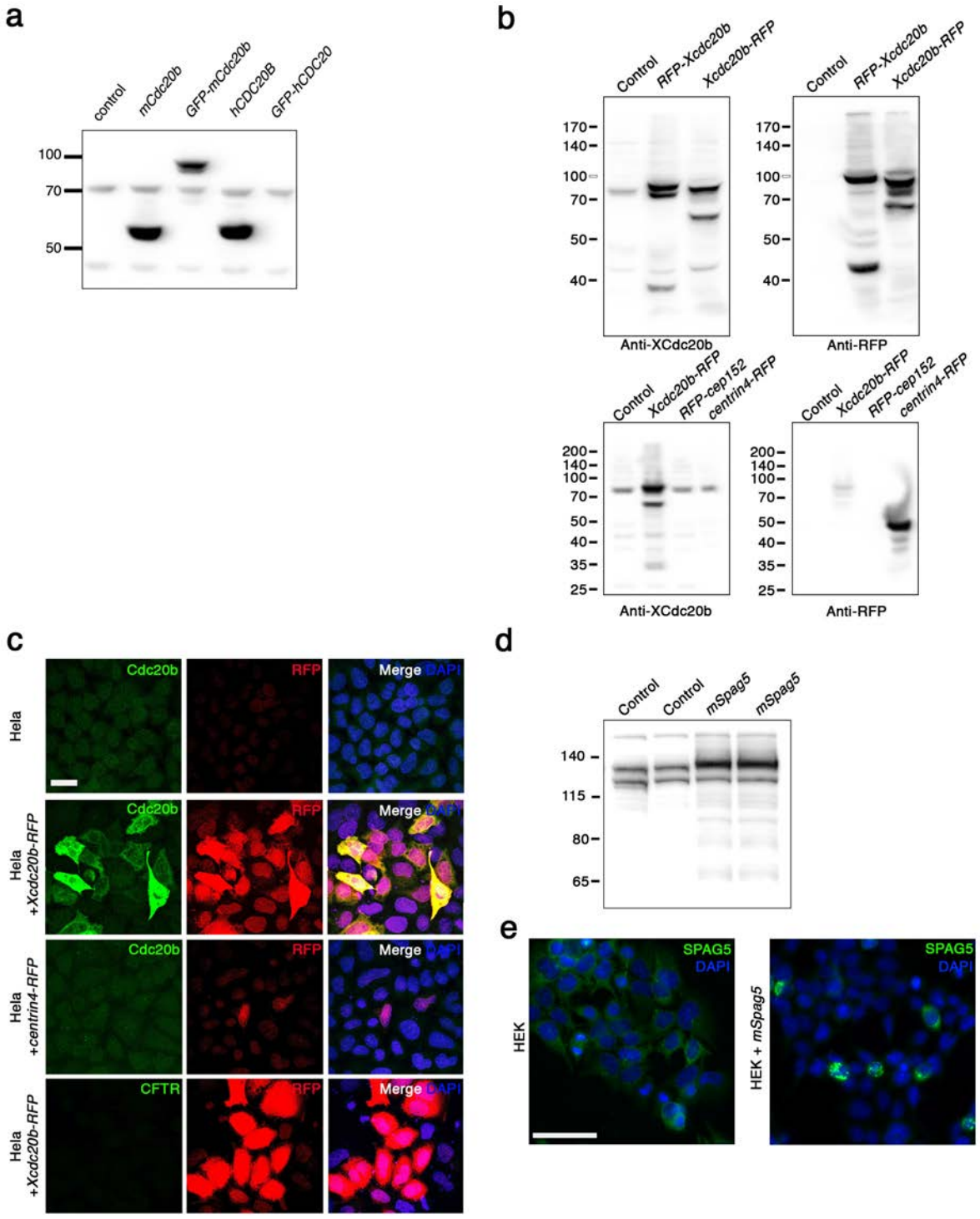

Supplementary Figure 3: Antibody validations

(a) COS1 cells were transfected with vectors coding for the indicated proteins and immunoblot was performed using Proteintech rabbit antibody raised against human CDC20B. This antibody recognized human and mouse CDC20B but did not cross-react with human CDC20. (**b**) Hela cells were transfected with vectors coding for the indicated proteins and immunoblot was

performed using a custom-made rabbit antibody raised against *Xenopus* CDC20B. (**c**) Hela cells were transfected with vectors coding for the indicated proteins and immunostainings were performed using the antibodies indicated on the photographs. Note that the antibody directed against *Xenopus* CDC20B did not cross-react with the centriole marker Centrin4. (**d**) HEK cells were transfected in duplicate with pCMV6-mSpag5, lysed 24 hours later and western blot was performed using proteintech rabbit polyclonal antibody raised against human SPAG5. (**e**) HEK cells were transfected with pCMV6-mSpag5, fixed with methanol 24 hours later and immunostained using proteintech rabbit polyclonal antibody raised against human SPAG5. This antibody cross-reacted with mouse SPAG5. Scale bars: 20µm (**c**), 50µm (**e**).

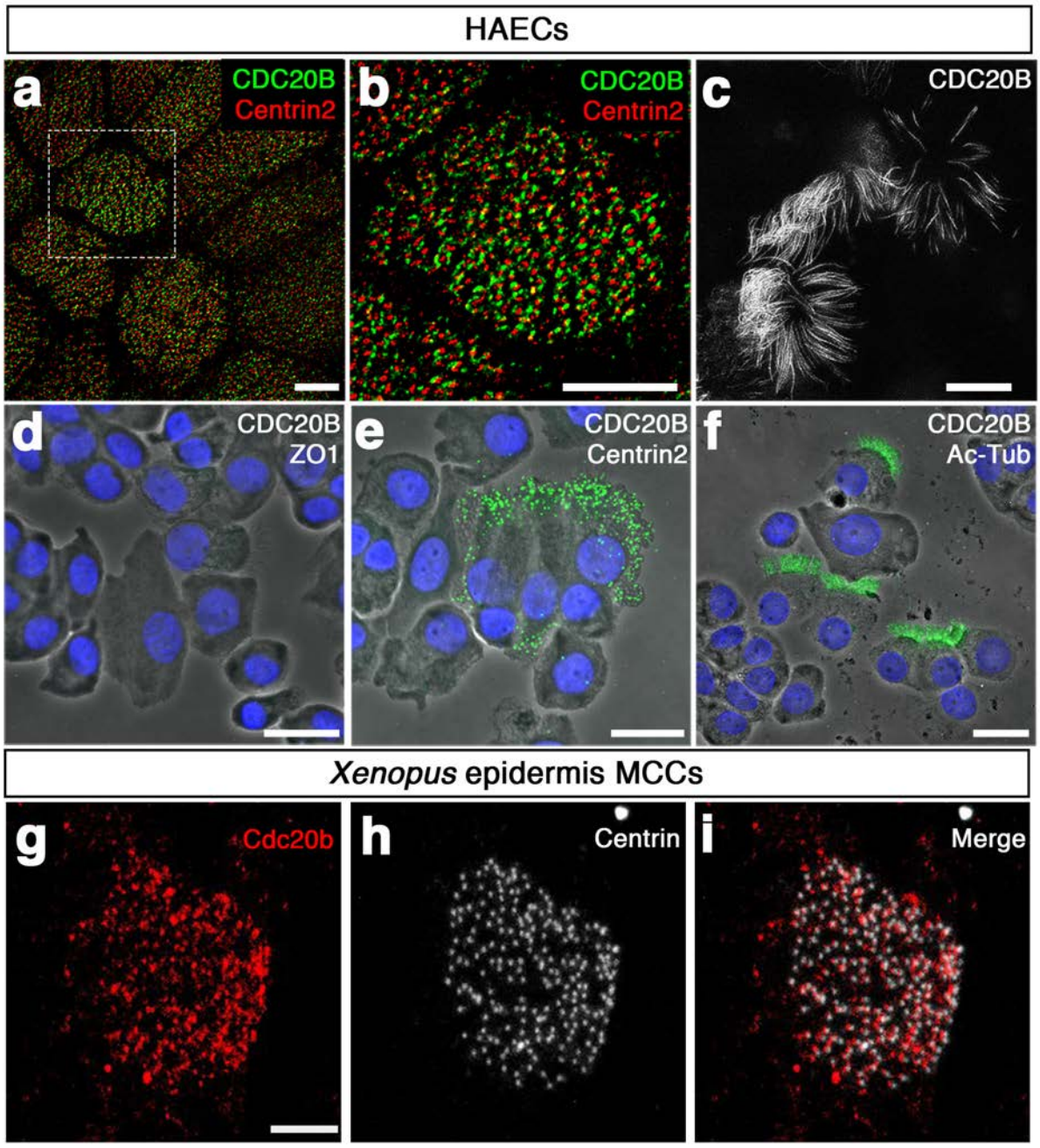

Supplementary Figure 4: CDC20B localization in mature MCCs.

(a-f) CDC20B sub-cellular localization in human mature MCCs. (a,**b**) ALI day 21 HAECs were fixed in methanol, and immunostained against CDC20B and Centrin2. STED super-resolution microscopy revealed the association of CDC20B to BBs. (**c**) ALI day 21 HAECs were fixed in paraformaldehyde, and immunostained against CDC20B. STED super-resolution microscopy revealed the association of CDC20B with cilia. (**d-f**) DuoLink Assays on fully

differentiated HAECs after cytospin. (**d**) Assay with CDC20B and ZO-1 antibodies was used as negative control. (**e**) Assay with CDC20B and Centrin2 (BBs) antibodies. (**f**) Assay with CDC20B and Acetylated-α-Tubulin (cilia) antibodies. Interaction between antibodies separated by less than 40nm generated green fluorescent signal. Nuclei are stained in blue. (**g-i**) **Cdc20b sub-cellular localization in *Xenopus* mature MCCs.** 4-cell *Xenopus* embryos were injected with *Multicilin-hGR* mRNA, induced with dexamethasone at stage 10.5 to activate Multicilin and immunostained for CDC20B (**g**) and Centrin (**h**) at stage 23. Scale bars: 5μm (**a-c**), 20μm (**d-f**), 5μm (**g**).

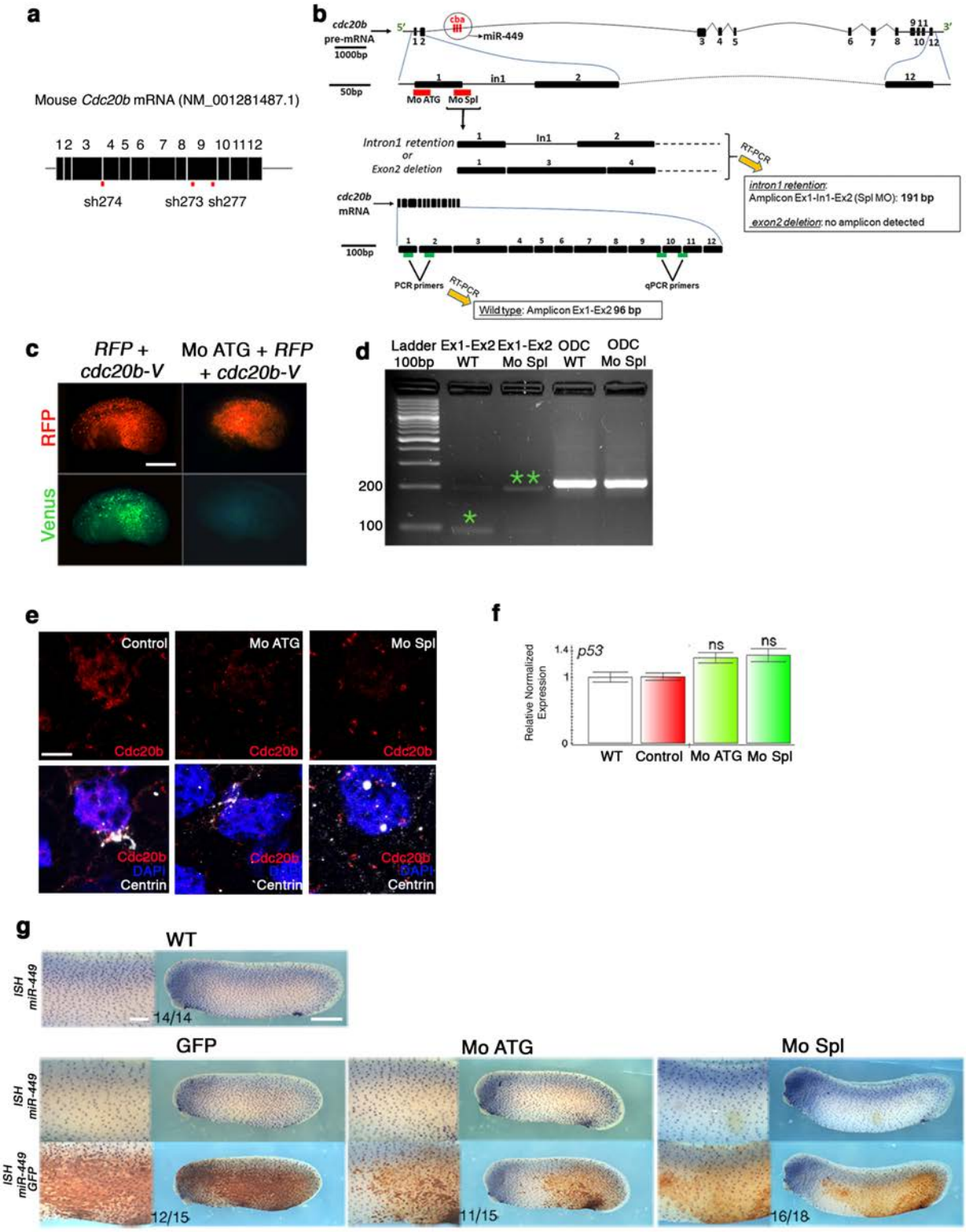

Supplementary Figure 5: *cdc20b* knockdown in mouse and *Xenopus*.

(**a**) Schematic representation of mouse *Cdc20b* mRNA and position of shRNAs used in this study. Note that sh274 targets the junction between exons 3 and 4, ruling out possible

interference with the production of miR-449 molecules from the *Cdc20b* pre-mRNA. (**b**) Schematic representation of *Xenopus cdc20b* pre-mRNA with introns, exons and miR-449abc relative position and size. Red horizontal bars below exon1 show the position of *cdc20b* Mo ATG and Mo Spl. On the bottom, green horizontal bars indicate RT-PCR and qPCR primer positions. (**c**) The efficiency of Mo ATG was verified through fluorescence extinction of co-injected *cdc20b-Venus*. (**d**) RT-PCR confirmed that Mo Spl caused intron1 retention (amplicon=191bp; double green stars), which is expected to introduce a premature stop codon and to produce a Cdc20b protein lacking 96% of its amino-acids, likely to undergo unfolded protein response-mediated degradation. (**e**) Immunostaining with the anti-*Xenopus* CDC20B antibody confirmed that both Mo ATG and Mo Spl severely down-regulated CDC20B protein expression in st18 MCCs. (**f**) RTqPCR revealed that neither *cdc20b* mopholinos caused significant *p53* transcript up-regulation, a non-specific response sometimes detected in zebrafish embryos subjected to morpholinos. Four independent experiments were carried out to check *p53* expression in morphant conditions. (**g**) miR-449 expression revealed by whole-mount *in situ* hybridization with LNA probes was not perturbed in the presence of either morpholinos. Embryos were photographed before (top) and after (bottom) staining against co-injected GFP-CAAX to be able to detect miR-449 staining. The number of embryos showing normal miR-449 expression over the total number of embryos analyzed is indicated on the photographs. Scale bars: 500µm (**c**), 5µm (**e**), 500µm (**g**, whole embryo), 80µm (**g**, zoom).

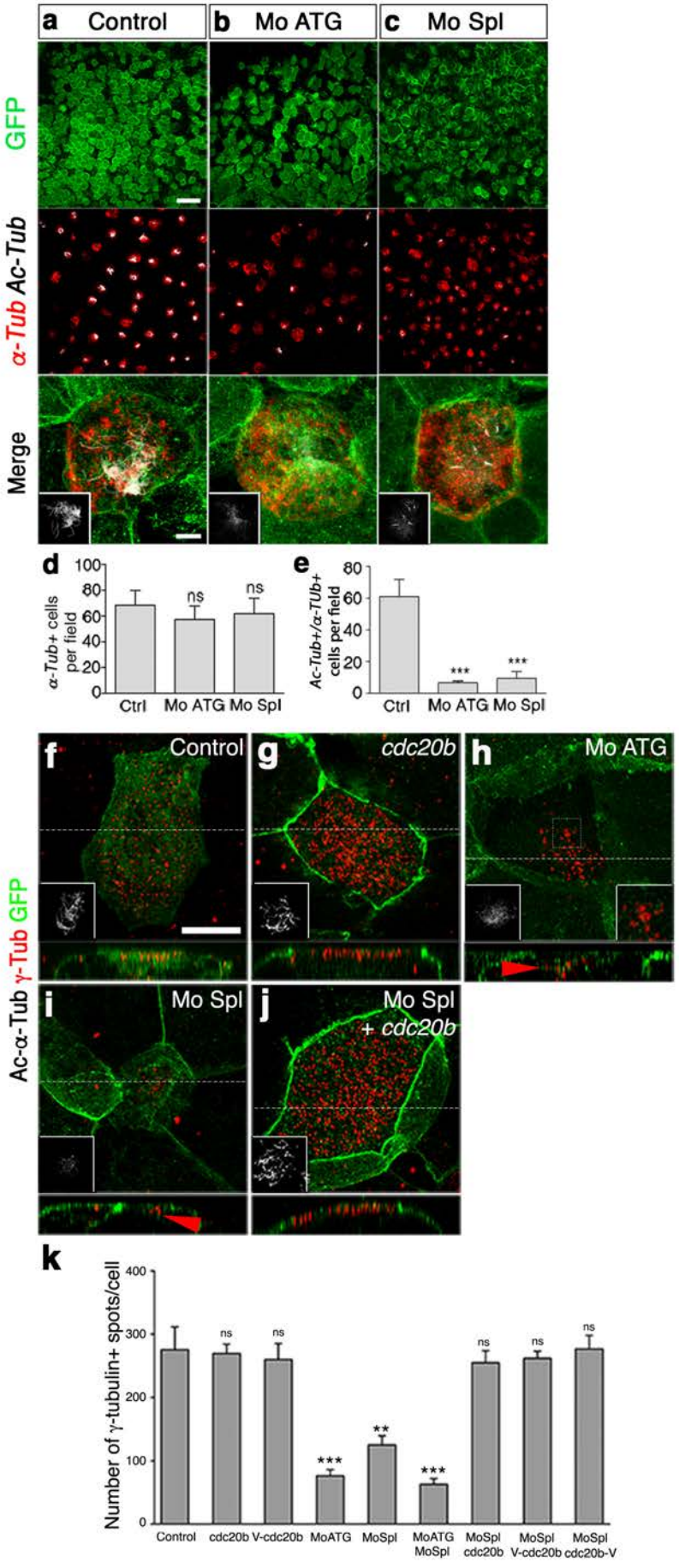
a Control
b Mo ATG
c Mo Spl
GFP
α-Tub Ac-Tub
Merge
d
α-Tub+ cells per field
ns
ns
Ctrl
Mo ATG
Mo Spl
e
Ac-Tub+/α-TUb+ cells per field
***
***
Ctrl
Mo ATG
Mo Spl
f Control
g cdc20b
h Mo ATG
Ac-α-Tub γ-Tub GFP
i Mo Spl
j Mo Spl + cdc20b
k
Number of γ-tubulin+ spots/cell
ns
ns
***
**
***
ns
ns
ns
Control
cdc20b
V-cdc20b
MoATG
MoSpl
MoATG MoSpl
MoSpl cdc20b
MoSpl V-cdc20b
MoSpl cdc20b-V

Supplementary Figure 6: *cdc20b* knockdown impairs multiciliogenesis in *Xenopus*.

(**a**-**e**) 8-cell embryos were injected in presumptive epidermis with *cdc20b* morpholinos and *GFP-CAAX* mRNA (injection tracer) as indicated. Control was provided by *GPF-CAAX* injection alone. Embryos at tailbud st25 were processed for fluorescent staining against GFP (green), Acetylated α-Tubulin (cilia, white) and *α-Tub* mRNA (MCC marker, red). Insets on merged panels show cilia staining. Note that *cdc20b* morphant MCCs maintain expression of fate marker *α-Tub* but poorly grow cilia. (**d**) Bar graph showing quantification of *α-Tub*/GFP double positive cells per field of observation. (**e**) Bar graph showing quantification of *α-Tub*/Ac-Tub/GFP triple positive cells per field of observation. 10 fields corresponding to 10 different embryos were analyzed for each condition. (**f**-**k**) 8-cell embryos were injected in presumptive epidermis with *cdc20b* morpholinos, *GFP-CAAX* and *cdc20b* mRNAs as indicated, and immunostained at tailbud st25 against GFP (injection tracer, green), γ-tubulin (BBs, red) and Acetylated α-Tubulin (cilia, white, left insets). Right inset in **h**: zoom on a stalled deuterosomal figure. z-projections made along white dotted lines are shown in bottom panels. Arrowheads point undocked BBs. (**k**) Bar graph showing the quantification of γ-tubulin spots per MCC. As two individual γ-tubulin spots are detected around each basal body, twice as many spots are usually counted as compared to Centrin (Fig. 5j-o). Note that BB numbers were restored to normal levels in *cdc20b* Spl morphants injected with tagged and untagged versions of *cdc20b*. Scale bars: 50µm (**a**, top), 5µm (**a**, bottom), 5µm (**f**).

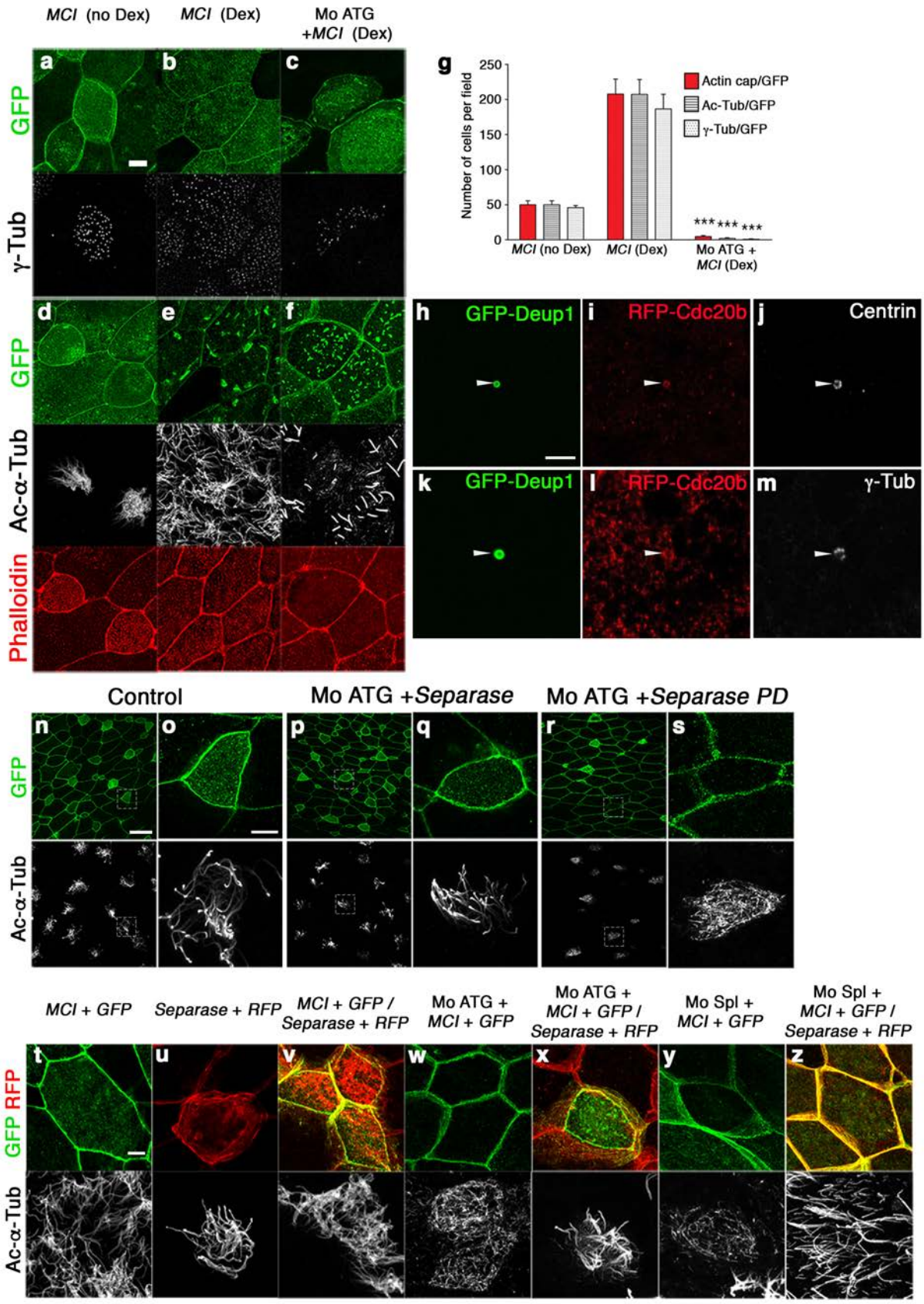

Supplementary Figure 7: *cdc20b* knockdown prevents multiciliogenesis induced by Multicilin, and is counteracted by Separase overexpression.

(**a**-**g**) ***cdc20b* knockdown prevents multiciliogenesis induced by Multicilin.** 8-cell embryos were injected in presumptive epidermis with *Multicilin-hGR* mRNA (*MCI*) and *cdc20b* Mo ATG, as indicated. *GFP-GPI* mRNA was co-injected as a tracer. MCI-hGR-injected embryos were induced with dexamethasone at st11. To check the efficiency of MCI induction some embryos were not treated with dexamethasone and served as controls (no DEX). Embryos were fixed at tailbud st25, and were stained against GFP (green) and γ-Tubulin (basal bodies, white)(**a**-**c**), or against GFP (green), phalloidin (apical actin, red), and Acetylated-α-Tubulin (cilia, white)(**d**-**f**). Note that *cdc20b* morphant MCI-induced MCCs failed to amplify centrioles, to maintain a proper actin cap, and to grow cilia. (**g**) Bar graph showing the quantification of GFP-positive cells that displayed normal actin, basal body and cilium staining. 5 fields (40x) per condition were analyzed. (**h**-**m**) **Deup1 recruits CDC20B in centriole amplification platforms.** 8-cell embryos were injected in presumptive epidermis with *Multicilin-hGR*, *RFP-CDC20B*, and *GFP-Deup1*mRNAs. Multicilin activity was induced with dexamethasone at st11, embryos were fixed at st18 and stained for GFP, RFP, Centrin (centrioles) or γ-Tubulin (deuterosome). White arrowheads point a centriole amplification platform positive for GFP-Deup1, which incorporates RFP-CDC20B, consistent with their capacity to form a complex (Fig. 6c). (**n**-**z**) **Wild-type but not protease-dead Separase rescues multiciliogenesis in MCCs deficient for Cdc20b.** (**n**-**s**) 8-cell embryos were injected in presumptive epidermis with *GFP-GPI* mRNA, human *Separase* mRNA, and *cdc20b* Mo ATG, as indicated. Immunofluorescence against GFP (injection tracer, green), and Acetylated-α-Tubulin (cilia, white) was performed at tailbud st25. Cells in dotted squares were blown up for better visualization. Note that multiciliogenesis was rescued in *cdc20b* morphant MCCs by wild-type (**p**,**q**) but not protease-dead Separase (**r**,**s**). (**t**-**z**) 4-cell embryos were injected in one ventral blastomere (presumptive epidermis) with *MCI-hGR* and *GFP-GPI* mRNAs, in the presence or not of *cdc20b* morpholinos, as indicated. Next, at 16-cell stage, half of those embryos were

injected with human *Separase* and RFP mRNAs in one ventral-animal blastomere. This setup was designed to avoid co-injection of *cdc20b* morpholinos with *Separase* mRNA, ruling out non-specific interference *in vitro* between these reagents. MCI-hGR-injected embryos were induced with dexamethasone at st11. All embryos were fixed at tailbud st25 and stained for GFP (*cdc20b* Mo tracer, green), RFP (*Separase* tracer, red) and Acetylated-α-Tubulin (cilia, white). Note that multiciliogenesis failed in MCI-induced *cdc20b* morphant MCCs (**w**,**y).** The presence of Separase rescued multiciliogenesis in MCI-induced *cdc20b* morphant MCCs (**x**,**z**). Scale bars: 5μm (**a**, **h**, **o**, **t**), 20μm (**n**).

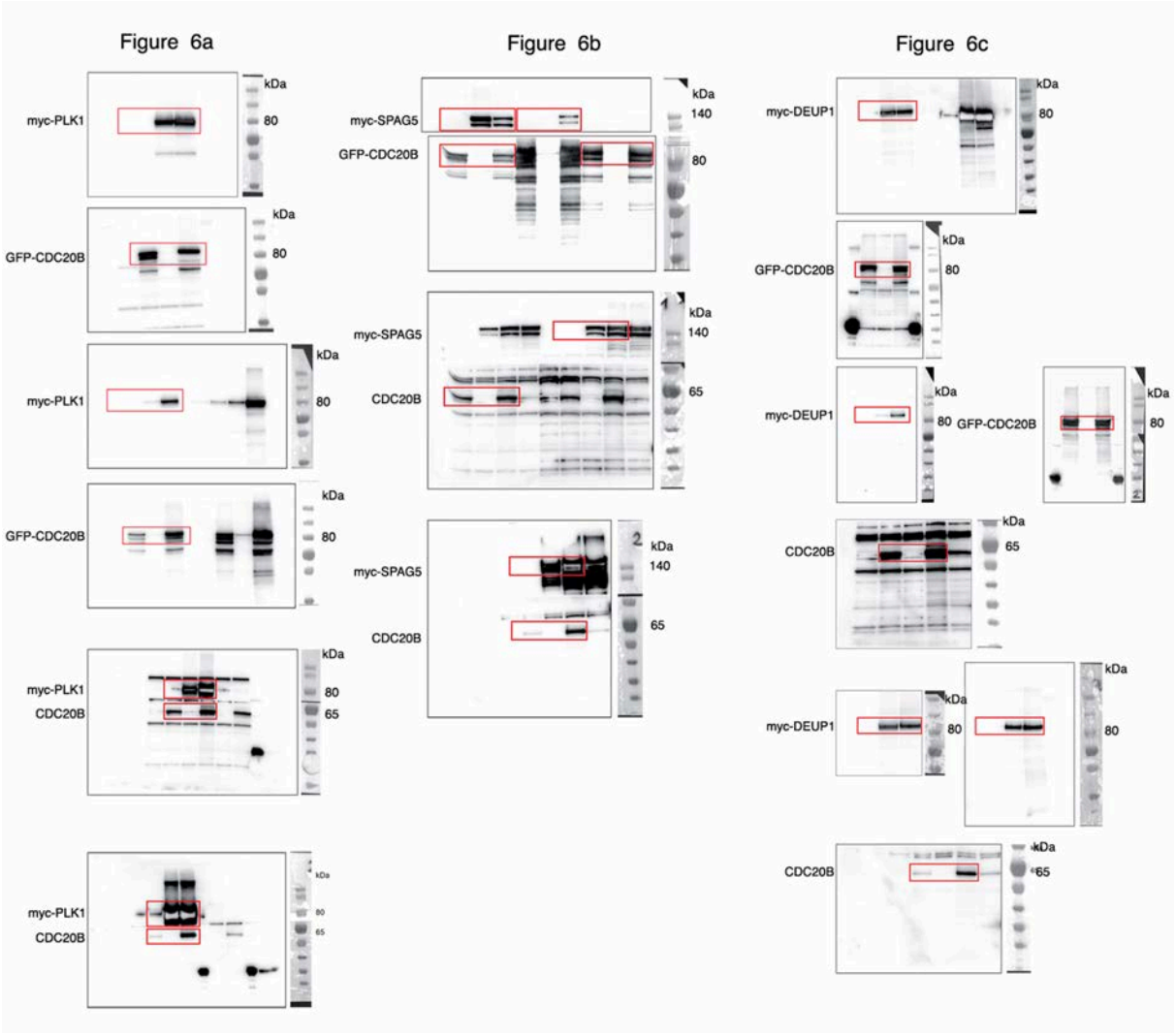

Supplementary Figure 8: Uncropped Western blots.

Red boxes mark the parts of the Western blot images that are shown in the indicated parts of Figure 6.

G1/S	
Symbol	Ensembl
ORC1	ENSG00000085840
ZNF367	ENSG00000165244
ADAMTS1	ENSG00000154734
CCNE2	ENSG00000175305
CDC25A	ENSG00000164045
RECQL4	ENSG00000160957
DTL	ENSG00000143476
CDC6	ENSG00000094804
CCNE1	ENSG00000105173
MCM2	ENSG00000073111
GINS3	ENSG00000181938
CHAF1B	ENSG00000159259
WDR76	ENSG00000092470
MCM6	ENSG00000076003
CLSPN	ENSG00000092853
CDCA7	ENSG00000144354
OSBPL6	ENSG00000079156
RAB23	ENSG00000112210
PLCXD1	ENSG00000182378
SKP2	ENSG00000145604
MDM1	ENSG00000111554
GINS2	ENSG00000131153
E2F1	ENSG00000101412
MCM5	ENSG00000100297
SNHG10	ENSG00000247092
HSF2	ENSG00000025156
UBR7	ENSG00000012963
RMI2	ENSG00000175643
NUP43	ENSG00000120253
ACD	ENSG00000102977
ZMYND19	ENSG00000165724
MSH2	ENSG00000095002
CDCA7L	ENSG00000164649
KIAA1586	ENSG00000168116
PMS1	ENSG00000064933
UNG	ENSG00000076248
KIAA1147	ENSG00000257093
POLD3	ENSG00000077514
ANKRD10	ENSG00000088448
CHAF1A	ENSG00000167670
BARD1	ENSG00000138376
INTS8	ENSG00000164941
APEX2	ENSG00000169188
ACYP1	ENSG00000119640
MRI1	ENSG00000037757
INSR	ENSG00000171105
TOPBP1	ENSG00000163781
FAM105B	ENSG00000154124
NPAT	ENSG00000149308
PCDH7	ENSG00000169851
GMNN	ENSG00000112312
RNPC3	ENSG00000185946
RNF113A	ENSG00000125352
FAM122A	ENSG00000187866
CAPN7	ENSG00000131375
TIPIN	ENSG00000075131
C14orf142	ENSG00000170270
LNPEP	ENSG00000113441
USP53	ENSG00000145390
PANK2	ENSG00000125779
VPS72	ENSG00000163159
DIS3	ENSG00000083520

S	
Symbol	Ensembl
ANKRD18A	ENSG00000273170
REEP1	ENSG00000068615
DEPDC7	ENSG00000121690
CDC7	ENSG00000097046
DNA2	ENSG00000138346
EXO1	ENSG00000174371
KDELC1	ENSG00000134901
ANKRD18A	ENSG00000180071
BRIP1	ENSG00000136492
PKMYT1	ENSG00000127564
CDC45	ENSG00000093009
C11orf82	ENSG00000165490
BLM	ENSG00000197299
RAD51	ENSG00000051180
CCDC150	ENSG00000144395
CDCA5	ENSG00000146670
CPNE8	ENSG00000139117
MCM8	ENSG00000125885
ESCO2	ENSG00000171320
GOLGA8B	ENSG00000215252
ASF1B	ENSG00000105011
FANCA	ENSG00000187741
INTS7	ENSG00000143493
POLA1	ENSG00000101868
FANCI	ENSG00000140525
RRM2	ENSG00000171848
TTLL7	ENSG00000137941
RAD51AP1	ENSG00000111247
KAT2B	ENSG00000114166
CHML	ENSG00000203668
BRCA1	ENSG00000012048
ABHD10	ENSG00000144827
TYMS	ENSG00000176890
PRIM1	ENSG00000198056
TTC31	ENSG00000115282
E2F8	ENSG00000129173
CENPQ	ENSG00000031691
PHTF1	ENSG00000116793
MASTL	ENSG00000120539
OSGIN2	ENSG00000164823
GOLGA8A	ENSG00000175265
PHTF2	ENSG00000006576
BBS2	ENSG00000125124
BMI1	ENSG00000168283
FEN1	ENSG00000168496
RMI1	ENSG00000178966
NSUN3	ENSG00000178694
KAT2A	ENSG00000108773
CENPM	ENSG00000100162
ZWINT	ENSG00000122952
ORC3	ENSG00000135336
KIAA1598	ENSG00000187164
BIVM	ENSG00000134897
DNAJB4	ENSG00000162616
CCDC84	ENSG00000186166
DCAF16	ENSG00000163257
NUP160	ENSG00000030066
RFC2	ENSG00000049541
CDKN2AIP	ENSG00000168564
UBE2T	ENSG00000077152
DHFR	ENSG00000228716
PTAR1	ENSG00000188647
RAD18	ENSG00000070950
OGT	ENSG00000147162
EZH2	ENSG00000106462
C5orf42	ENSG00000197603
LYRM7	ENSG00000186687
CCDC14	ENSG00000175455
NAB1	ENSG00000138386
SP1	ENSG00000185591
RPA2	ENSG00000117748
RBBP8	ENSG00000101773
RRM1	ENSG00000167325
FAM178A	ENSG00000119906
SAP30BP	ENSG00000161526
NT5DC1	ENSG00000178425
CERS6	ENSG00000172292
ZBED5	ENSG00000236287
MAP3K2	ENSG00000169967

G2/M	
Symbol	Ensembl
IQGAP3	ENSG00000183856
TRAIP	ENSG00000183763
CDC25C	ENSG00000158402
NEIL3	ENSG00000109674
PIF1	ENSG00000140451
KIFC1	ENSG00000237649
HJURP	ENSG00000123485
NCAPH	ENSG00000121152
KIF23	ENSG00000137807
SKA3	ENSG00000165480
KIAA1524	ENSG00000163507
NDC80	ENSG00000080986
CCNF	ENSG00000162063
CDCA8	ENSG00000134690
PSRC1	ENSG00000134222
FANCD2	ENSG00000144554
ESPL1	ENSG00000135476
CDR2	ENSG00000140743
AURKB	ENSG00000178999
BORA	ENSG00000136122
LMNB1	ENSG00000113368
TRIM59	ENSG00000213186
CHEK2	ENSG00000183765
MND1	ENSG00000121211
CDCA2	ENSG00000184661
CKAP2L	ENSG00000169607
STIL	ENSG00000123473
POLQ	ENSG00000051341
MELK	ENSG00000165304
CENPL	ENSG00000120334
LIX1L	ENSG00000152022
KIF11	ENSG00000138160
C14orf80	ENSG00000185347
UBE2C	ENSG00000175063
NCAPD3	ENSG00000151503
HAUS8	ENSG00000131351
FAM83D	ENSG00000101447
CDK1	ENSG00000170312
MAD2L1	ENSG00000164109
GABPB1	ENSG00000104064
SAP30	ENSG00000164105
CFD	ENSG00000197766
TTF2	ENSG00000116830
MID1	ENSG00000101871
GAS1	ENSG00000180447
TUBA1A	ENSG00000167552
ZNF587	ENSG00000198466
TUBD1	ENSG00000108423
FAN1	ENSG00000198690
CDKN2C	ENSG00000123080
TUBB2A	ENSG00000137267
TNPO2	ENSG00000105576
ZNHIT2	ENSG00000174276
TRMT2A	ENSG00000099899
PKNOX1	ENSG00000160199
ENTPD5	ENSG00000187097
KDM4A	ENSG00000066135
STK17B	ENSG00000081320
KLF6	ENSG00000067082
KATNA1	ENSG00000186625
H2AFX	ENSG00000188486
BRD8	ENSG00000112983
RCCD1	ENSG00000166965
CDKN1B	ENSG00000111276
UACA	ENSG00000137831
KCTD9	ENSG00000104756
ATL2	ENSG00000119787
KPNA2	ENSG00000182481
HRSP12	ENSG00000132541
VTA1	ENSG00000009844
HMGB2	ENSG00000164104
C2orf69	ENSG00000178074
FADD	ENSG00000168040
HIPK2	ENSG00000064393
KIF22	ENSG00000079616
MGAT2	ENSG00000168282
NR3C1	ENSG00000113580
DHX8	ENSG00000067596
NMB	ENSG00000197696
TFAP2A	ENSG00000137203
HINT3	ENSG00000111911
CDC16	ENSG00000130177
NUMA1	ENSG00000137497
ARMC1	ENSG00000104442
STAT1	ENSG00000115415
CCDC107	ENSG00000159884
TMPO	ENSG00000120802

M	
Symbol	Ensembl
CKS1B	ENSG00000268942
DEPDC1B	ENSG00000035499
SHCBP1	ENSG00000171241
FAM64A	ENSG00000129195
FYN	ENSG00000010810
KIF2C	ENSG00000142945
SPAG5	ENSG00000076382
CIT	ENSG00000122966
CENPA	ENSG00000115163
DIAPH3	ENSG00000139734
CADM1	ENSG00000182985
KIF14	ENSG00000118193
PLK1	ENSG00000166851
MDC1	ENSG00000137337
DEPDC1	ENSG00000024526
BUB1	ENSG00000169679
DLGAP5	ENSG00000126787
NUF2	ENSG00000143228
CEP55	ENSG00000138180
GTSE1	ENSG00000075218
HMMR	ENSG00000072571
FOXM1	ENSG00000111206
E2F5	ENSG00000133740
PRR11	ENSG00000068489
NEK2	ENSG00000117650
TACC3	ENSG00000013810
CENPE	ENSG00000138778
CCNB2	ENSG00000157456
CDC20	ENSG00000117399
BIRC5	ENSG00000089685
CCDC88A	ENSG00000115355
POC1A	ENSG00000164087
MKI67	ENSG00000148773
MKI67	ENSG00000148773
HSPA13	ENSG00000155304
CDC25B	ENSG00000101224
TPX2	ENSG00000088325
AURKA	ENSG00000087586
ANKRD40	ENSG00000154945
CENPF	ENSG00000117724
CNTROB	ENSG00000170037
NCAPD2	ENSG00000010292
SGOL2	ENSG00000163535
SRF	ENSG00000112658
DZIP3	ENSG00000198919
ECT2	ENSG00000114346
ORAOV1	ENSG00000149716
NUP35	ENSG00000163002
PTPN9	ENSG00000169410
HS2ST1	ENSG00000153936
RCAN1	ENSG00000159200
SS18	ENSG00000141380
HCFC1	ENSG00000172534
NUP98	ENSG00000110713
POM121	ENSG00000196313
TOMM34	ENSG00000025772
CKAP5	ENSG00000175216
GRK6	ENSG00000198055
SEPHS1	ENSG00000086475
QRICH1	ENSG00000198218
AHI1	ENSG00000135541
CNOT10	ENSG00000182973
KLF9	ENSG00000119138
SETD8	ENSG00000183955
ATF7IP	ENSG00000171681
RAD51C	ENSG00000108384
CDC42EP1	ENSG00000128283
HPS4	ENSG00000100099
GOT1	ENSG00000120053
MZT1	ENSG00000204899
RRP1	ENSG00000160214
AKIRIN2	ENSG00000135334
CDC27	ENSG00000004897
SMARCD1	ENSG00000066117
BIRC2	ENSG00000110330

M/G1	
Symbol	Ensembl
TROAP	ENSG00000135451
CDKN3	ENSG00000100526
PRC1	ENSG00000198901
HSD17B11	ENSG00000198189
BTBD3	ENSG00000132640
SLC39A10	ENSG00000196950
GTF3C4	ENSG00000125484
WWC1	ENSG00000113645
ELP3	ENSG00000134014
FOXK2	ENSG00000141568
OPN3	ENSG00000054277
KIAA0586	ENSG00000100578
ANTXR1	ENSG00000169604
CEP70	ENSG00000114107
HMGCR	ENSG00000113161
TULP4	ENSG00000130338
ZNF281	ENSG00000162702
CDK7	ENSG00000134058
LYAR	ENSG00000145220
PPP6R3	ENSG00000110075
DCP1A	ENSG00000162290
FAM189B	ENSG00000160767
AGPAT3	ENSG00000160216
PSEN1	ENSG00000080815
NUP37	ENSG00000075188
MSL1	ENSG00000188895
AGFG1	ENSG00000173744
SNUPN	ENSG00000169371
STAG1	ENSG00000118007
LRIF1	ENSG00000121931
PAK1IP1	ENSG00000111845
NCOA3	ENSG00000124151
PTTG1	ENSG00000164611
CTR9	ENSG00000198730
DKC1	ENSG00000130826
FOPNL	ENSG00000133393
VCL	ENSG00000035403
MRPS2	ENSG00000122140
WIPF2	ENSG00000171475

Supplementary Table 1: Gene sets used to assess enrichment of cell cycle phases related transcripts in individual cells analyzed by scRNA-seq.

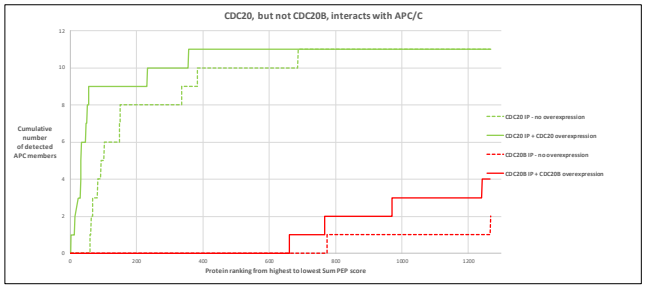

Protein ranking from highest to lowest Sum PEP score	Cumulative number of detected APC/C members			
	CDC20 IP - no overexpression	CDC20 IP + CDC20 overexpression	CDC20B IP - no overexpression	CDC20B IP + CDC20B overexpression
1	0	0	0	0
2	0	1	0	0
6	0	1	0	0
7	0	1	0	0
12	0	1	0	0
13	0	2	0	0
24	0	3	0	0
27	0	3	0	0
28	0	3	0	0
30	0	3	0	0
31	0	4	0	0
32	0	5	0	0
33	0	6	0	0
46	0	6	0	0
47	0	7	0	0
50	0	7	0	0
51	0	8	0	0
55	0	8	0	0
56	0	9	0	0
59	0	9	0	0
60	1	9	0	0
62	1	9	0	0
63	2	9	0	0
67	2	9	0	0
68	3	9	0	0
81	3	9	0	0
82	4	9	0	0
91	4	9	0	0
92	5	9	0	0
101	5	9	0	0
102	6	9	0	0
147	6	9	0	0
148	7	9	0	0
149	7	9	0	0
150	8	9	0	0
231	8	9	0	0
232	8	10	0	0
335	8	10	0	0
336	9	10	0	0
356	9	10	0	0
357	9	11	0	0
382	9	11	0	0
383	10	11	0	0
660	10	11	0	0
661	10	11	0	1
685	10	11	0	1
686	11	11	0	1
767	11	11	0	1
768	11	11	0	2
773	11	11	0	2
774	11	11	1	2
970	11	11	1	2
971	11	11	1	3
1241	11	11	1	3
1242	11	11	1	4
1265	11	11	1	4
1266	11	11	2	4

IP CDC20 - no overexpression

Protein FDR Confidence	Accession	Symbol	Description	Sum PEP Score	Coverage	# Peptides	# PSMs	# Unique Peptides	MW [kDa]	emPAI	Score Sequest HT	global rank	APC rank
High	Q9UJX2	CDC23	Cell division c	109,78	47,74	27	48	27	68,79	6,80	88,85	60	1,00
High	**Q12834**	**CDC20**	**Cell division c**	**104,51**	**49,70**	**16**	**56**	**16**	**54,69**	**10,94**	**158,30**	63	2,00
High	Q9H1A4	ANAPC1	Anaphase-pro	101,92	23,66	32	42	32	216,36	1,30	36,79	68	3,00
High	Q9UJX4	ANAPC5	Anaphase-pro	91,89	42,38	23	50	23	85,02	3,19	83,00	82	4,00
High	Q9UJX3;A0A024RBJ3	ANAPC7	Anaphase-pro	85,18	46,58	21	38	21	66,81	6,13	61,05	92	5,00
High	A0A024RD22;Q13042	CDC16	CDC16 cell div	79,32	43,55	21	31	21	71,61	4,37	48,14	102	6,00
High	P30260	CDC27	Cell division c	63,63	26,33	16	31	1	91,81	2,00	41,46	148	7,00
High	G5EA36	CDC27	Cell division c	63,28	26,25	16	31	1	91,68	2,00	41,49	150	8,00
High	Q9UJX6	ANAPC2	Anaphase-pro	37,09	22,75	13	15	13	93,77	0,93	15,24	336	9,00
High	Q9UJX5	ANAPC4	Anaphase-pro	31,69	16,34	13	13	13	92,06	0,89	7,67	383	10,00
High	Q9UM13	ANAPC10	Anaphase-pro	16,01	31,89	5	9	5	21,24	1,85	11,56	686	11,00

IP CDC20 + CDC20 overexpression

Protein FDR Confidence	Accession	Symbol	Description	Sum PEP Score	Coverage	# Peptides	# PSMs	# Unique Peptides	MW [kDa]	emPAI	Score Sequest HT	global rank	APC rank
High	Q9H1A4	ANAPC1	Anaphase-pro	710,46	59,57	81	319	81	216,36	28,94	640,59	2	1
High	Q9UJX4	ANAPC5	Anaphase-pro	463,89	66,23	50	288	46	85,02	142,07	635,28	13	2
High	Q9UJX5	ANAPC4	Anaphase-pro	371,59	59,53	43	198	43	92,06	34,74	384,67	24	3
High	**Q12834**	**CDC20**	**Cell division c**	**332,93**	**69,54**	**28**	**791**	**28**	**54,69**	**202,09**	**1712,61**	28	3
High	P30260	CDC27	Cell division c	306,64	60,56	34	215	1	91,81	20,92	435,97	31	4
High	G5EA36	CDC27	Cell division c	306,44	60,51	34	212	1	91,68	20,92	426,79	32	5
High	Q9UJX6	ANAPC2	Anaphase-pro	301,10	54,50	45	165	45	93,77	27,12	297,57	33	6
High	A0A024RD22;Q13042	CDC16	CDC16 cell div	253,91	55,00	29	108	29	71,61	22,90	226,42	47	7
High	Q9UJX2	CDC23	Cell division c	244,49	54,77	33	121	33	68,79	27,80	262,31	51	8
High	Q9UJX3;A0A024RBJ3	ANAPC7	Anaphase-pro	236,24	64,61	32	117	32	66,81	37,75	239,65	56	9
High	Q9UM13	ANAPC10	Anaphase-pro	86,65	76,22	11	43	11	21,24	27,48	98,76	232	10
High	I3L3H6	CDC27	Cell division c	63,60	63,09	7	32	1	25,91	5,81	75,14	357	11

IP CDC20 B-no overexpression

Protein FDR Confidence	Accession	Symbol	Description	Sum PEP Score	Coverage	# Peptides	# PSMs	# Unique Peptides	MW [kDa]	emPAI	Score Sequest HT	global rank	APC rank
High	Q9UJX5	ANAPC4	Anaphase-pro	7,09	3,47	1	2	1	92,06	0,05	2,13	774	1
High	A0A024RD22;Q13042	CDC16	CDC16 cell div	2,31	4,68	1	1	1	71,61	0,06	0,00	1266	2

IP CDC20 B + CDC20B overexpression

Protein FDR Confidence	Accession	Symbol	Description	Sum PEP Score	Coverage	# Peptides	# PSMs	# Unique Peptides	MW [kDa]	emPAI	Score Sequest HT	global rank	APC rank
High	**Q86Y33**	**CDC20B**	**Cell division c**	**215,12**	**60,89**	**26**	**271**	**26**	**57,30**	**41,99**	**546,93**	7	0
High	Q9UJX2	CDC23	Cell division c	11,98	12,90	5	5	5	68,79	0,37	0,00	661	1
High	A0A024RD22;Q13042	CDC16	CDC16 cell div	9,77	5,65	3	3	3	71,61	0,21	3,53	768	2
High	P30260	CDC27	Cell division c	6,89	3,64	3	3	3	91,81	0,17	3,63	971	3
High	Q9UJX3;A0A024RBJ3	ANAPC7	Anaphase-pro	4,21	6,18	2	2	2	66,81	0,15	0,00	1242	4

Supplementary Table 2: CDC20, but not CDC20B, interacts with APC/C.